Interaction pressure tensor on high-order lattice Boltzmann models for nonideal fluids

C. S. From,[1,*] E. Sauret,[1,†] S. A. Galindo-Torres,[2,3] and Y. T. Gu[1]

[1]*Laboratory for Advanced Modelling and Simulation in Engineering and Science, School of Chemistry, Physics, and Mechanical Engineering, Science and Engineering Faculty, Queensland University of Technology, Queensland 4001, Australia*
[2]*Department of Civil Engineering and Industrial Design, University of Liverpool, Liverpool L69 3BX, United Kingdom*
[3]*School of Engineering, Westlake University, Hangzhou, Zhejiang Province 310024, China*

In this work we address the application of pseudopotentials directly on high-order lattice Boltzmann models. We derive a general expression for the pressure tensor on high-order lattices considering all nonideal interactions, including intra- and intermolecular interactions, following the discrete lattice theory introduced by X. Shan [Phys. Rev. E **77**, 066702 (2008)]. From the derived expression, a generalized continuum approximation, truncated at fourth-order isotropy, is obtained that is readily applicable to high-order lattices. With this, we demonstrate that high-order lattice models with pseudopotentials can satisfy thermodynamic consistency. The derived generalized expression and continuum approximation are validated for the case of a flat interface and compared against the standard definition available from the literature. The generalized expression is also shown to accurately reproduce the Laplace experiment for a variety of high-order lattice structures. This work sets the preliminary steps towards the application of high-order lattice models for simulating nonideal fluid mixtures.

I. INTRODUCTION

Microscopic fluid dynamic problems often involve various processes including mixing, separation, and sorting of cells and particles in heterogeneous mediums, at high throughputs [1,2]. Many of these applications involve fluid mixtures, a system composed of various species and/or phases. The inclusion of various phases and/or species results in the fluid, as a whole, deviating from the conventional ideal-fluid definition (where competing interactions are absent). Understanding the physical phenomenon at the microscopic scale is still limited despite the well-established advantages of potential applications, such as microfluidic devices [1]. Computational methods have the ability to describe such a phenomenon and provide a detailed description of transport properties that are not observable and quantifiable through experimentation [3,4]. The challenge facing computational modeling of the various microscopic fluid dynamic systems is the inclusion of multiple components and their intra- and intermolecular interactions.

The lattice Boltzmann (LB) method has recently gained tremendous popularity, with potential qualities that are attractive to microscopic fluid dynamics including accuracy, adaptability [5], and scalable parallel computations [6]. The LB method is also an attractive alternative to Navier-Stokes (NS) based numerical methods for simulating microfluidic applications [3,5,7]. Shan *et al.* [8] demonstrated that higher-order LB models have the ability to describe hydrodynamics that is beyond Navier-Stokes capabilities [8,9]. Therefore, the LB method has the potential to be used as an alternative to

computationally expensive atomistic methods such as direct simulation Monte Carlo [10]. For fluid flow problems where Knudsen numbers (Kn) are near unity, a description of hydrodynamics that is beyond the NS representation is required and is achieved through high-order expansions of the LB equilibrium distribution function, $M > 3$. As the general rule for matching the order (M) of equilibrium distribution to the algebraic degree (N) of precision of the lattice structure is $N > 2M$ [8,11], these flow problems subsequently require a larger lattice structure [8,10]. More methodological details, theoretical proof, and more insights into the methods of choosing orders and corresponding lattice structures can be found in [8,9].

Extensions to the LB method allow nonideal fluids to be simulated where these extensions are in general based on the free energy [12] and pseudopotential interactions [13]. Recent development of the entropic LB (ELB) method, proposed almost two decades ago in [14,15], have the potential to extend the capabilities of the LB method to model complex systems including turbulent flow [16] and nonideal fluids as shown in recent works [17,18] using the free-energy model. In this work we are interested in the pseudopotential model first introduced by Shan and Chen [13], generally referred to as the Shan-Chen (SC) model, which has consistently been shown to accurately reproduce complex multicomponent systems [19–23] including sliding droplets on chemical surfaces [24,25]. It was also shown in [26] that it is possible to combine the ELB method with the SC model. The advantage of the SC model is that it allows intra- and intermolecular interactions to be modeled directly. More specifically, the SC model depicts these interactions by a pseudopotential ψ (a function of local density) and an amplitude $\mathcal{G}$. For this reason, transport properties are directly related to ψ and $\mathcal{G}$; a direct link to the macroscopic fluid equations can be derived

———————
*christopher.from@hdr.qut.edu.au
†emilie.sauret@qut.edu.au

using the Chapman-Enskog analysis as shown by the inventors Shan and Chen [13] in their succeeding works [27–29]. This analysis requires knowledge of the interaction pressure tensor, which, in a nonideal fluid, depends on the competing interactions [30]. The pressure tensor is also required to describe the dynamics at the fluid interface [31–34]. Despite theoretical advancements of LB models and pseudopotentials, limited work addresses pseudopotentials for high-order LB single- and multicomponent models. We believe that one contributing factor is the difficulties in successful application of pseudopotentials with higher-order lattice models, which is likely the result of the undefined form of the interaction pressure tensor.

A pioneering work by Shan [32], using a forcing model with a lattice structure that conforms with eighth-order-isotropy gradients, demonstrated that the consequent interaction pressure tensor is dependent on the lattice structure. Shan [32] introduced this discrete theory to describe the pressure tensor by considering its very basic fundamental definition, i.e., the momentum flux through an area element. From this point of view, all force vectors directly *on the lattice* through an infinitesimal area **A** in space *x* will produce a consequent pressure tensor that in principle can be defined in a discrete form

$$\sum \boldsymbol{P} \cdot \mathbf{A} = -\sum_{x} \boldsymbol{F}, \tag{1}$$

where the increase in interaction length or number of interactions links, or both, will result in an increased number of force vectors passing through **A**. Hence, depending on the lattice structure, different contributions to the interaction pressure tensor are to considered.

The long-wavelength limit of Eq. (1) is defined by its continuum differential form

$$\nabla \cdot \boldsymbol{P} = -\boldsymbol{F}, \tag{2}$$

which can be used to define the continuum link between the interaction force and subsequent pressure tensor. That is, to define the interaction pressure tensor in space *x* the differential form (2) requires only the knowledge of the interaction force equation alone, whereas the discrete definition (1) is derived directly on the lattice structure and requires the exact knowledge of the contribution from all force vectors passing through **A** in space *x*. Clearly, the differential form is significantly more convenient to obtain and, since the form of the interaction force equation is not dependent on the lattice, has the same solution for any lattice model. In the limited literature where pseudopotentials are applied on high-order lattice models, including [26] and more recently [35], the differential form [Eq. (2)] is used to describe the interaction pressure tensor. The same was done in [30], which used the same eighth-order-isotropy lattice as in [32]. However, as shown in [32,34,36], even on the two-dimensional nine-velocity lattice model (D2Q9), the derived interaction pressure tensor from the discrete definition in Eq. (1) is inconsistent with the expression derived from Eq. (2). It was also noted in [30] that the exact lattice theory exists and could allow for more accurate calculation of the total momentum flux tensor. A continuum description of the interaction pressure tensor is still desirable, as it is more computationally and mathematically convenient, allowing the user to define the relevant transport

properties prior to simulations and thus allowing more precise control of the model [23]. As shown by Shan [32], with the exact discrete definition, a continuum approximation of the interaction pressure tensor can be obtained by approximating spatial derivatives. In essence, in order for such a solution to be derived for higher-order lattices, the exact discrete definition of the interaction pressure tensor, based on Eq. (1), has to be defined first. Evidently, the discrete definition (1) is paramount for the application of SC pseudopotentials on high-order lattice models. So far, the eighth-order-isotropy force interaction model used by Shan [32] originally is the only lattice structure available in the literature with an exact discrete definition.

Our work aims to provide a general and programmable expression of the interaction pressure tensor for higher-order lattices in line with the discrete definition in Eq. (1) that includes all forms of interactions required in microscopic fluid dynamic systems, including intra- and intermolecular interactions.

The paper is structured as follows. In Sec. II we introduce the general lattice Boltzmann method for nonideal fluids including the high-order equilibrium distribution function. In Sec. III we derive the general expression for the discrete interaction pressure tensor for high-order lattice structures. We then conduct the continuum analysis in Sec. IV and obtain a generalized solution for the continuum approximation truncated at fourth-order isotropy. The thermodynamic consistency is demonstrated for a single-component liquid-gas system in Sec. IV A. In addition, the surface tension coefficient is obtained in Sec. IV B. Numerical experiments and a discussion are provided in Sec. V. Finally, conclusions are drawn and a future outlook is given in Sec. VI.

II. LATTICE BOLTZMANN MODEL FOR NONIDEAL FLUIDS

In the lattice Boltzmann method, the mesoscopic representation of fluid flow is described by the distribution function f. In this work an athermal third-order $M = 3$ equilibrium distribution function (third-order Hermite polynomial expansion) is developed following the seminal work in [8] to recover the NS level of description of hydrodynamics, more specifically, the momentum dynamics and pressure tensor. This equilibrium distribution function is then projected on a two-dimensional high-order (multispeed) lattice structure. These two elements combined form the high-order lattice model. This work focuses on the general application of nonideal fluid using high-order lattices, with an example of such a lattice structure, denoted by Q49ZOTT [37], illustrated in Fig. 1 (details provided in Appendix A). Note that Q49ZOTT can recover up to a fourth-order equilibrium distribution [37] but is not required for the purposes of our work here and therefore is neglected. The Q49ZOTT structure is used here purely for demonstrative purposes, which will become apparent later in Sec. III.

In a nonideal fluid mixture system, consisting of a number S of components, each unique component is defined by its own lattice distribution f in space x, in each discrete velocity $\boldsymbol{\xi}_\alpha$ of all directions $\boldsymbol{\xi}_\alpha : \alpha = 0, \ldots, Q$, at time t. One
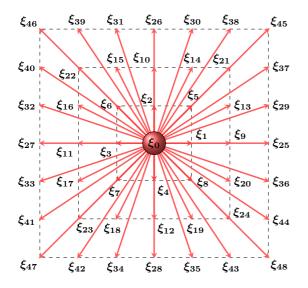
FIG. 1. Two-dimensional high-order lattice model constructed from projection of D1Q7 [37], i.e., a total of $7^2 = 49$ lattice velocities. We denote this lattice structure by Q49ZOTT, based on its D1Q7 construction on zero-one-two-three (ZOTT) velocity, analogous to the zero-one-three (ZOT) construction used for D2Q25ZOT in [37]. Refer to Appendix A for details.

component ϕ has the evolution

$$f_\alpha^\phi(\boldsymbol{x} + \boldsymbol{\xi}_\alpha, t + \Delta t) = f_\alpha^\phi(\boldsymbol{x}, t) - \Omega_\alpha^\phi + \Delta t S_\alpha^\phi(\boldsymbol{x}, t). \quad (3)$$

The left-hand side term $f_\alpha^\phi(\boldsymbol{x} + \boldsymbol{\xi}_\alpha, t + \Delta t)$ is the constant propagation of particles in space $\boldsymbol{x}$ at each time interval Δt. This direct and exact advection of particles, known as the streaming step, ensures that zero numerical diffusion is generated. This is a clear advantage compared to finite-difference (or finite-volume) schemes constructed on the basis of fractional advection. On the far right-hand side of Eq. (3) is the source term $S_\alpha^\phi(\boldsymbol{x}, t)$, which allows a force contribution $\boldsymbol{F}$ (such as the nonideal interactions and influences from external sources) to be included in the collision process. This is coupled explicitly with the distribution function to conserve the explicit nature of the LB method in [21,38],

$$S_\alpha^\phi = \frac{\boldsymbol{F}^\phi(\boldsymbol{\xi}_\alpha - \boldsymbol{u}^{\mathrm{eq}})}{\rho^\phi c_s^2} f_\alpha^{\mathrm{eq},\phi}, \quad (4)$$

where the collision term Ω_α^ϕ in Eq. (3),

$$\Omega_\alpha^\phi = \omega^\phi \left[f_\alpha^\phi(\boldsymbol{x}, t) + \frac{\Delta t}{2} S_\alpha^\phi(\boldsymbol{x}, t) - f_\alpha^{\mathrm{eq},\phi}(\boldsymbol{x}, t) \right], \quad (5)$$

relaxes the distribution using the relaxation parameter $\omega^\phi = 1/\tau^\phi$ based on the kinematic viscosity ν of the fluid, i.e., $\nu^\phi = c_s^2(\tau^\phi - \frac{1}{2})\frac{\Delta x^2}{\Delta t}$, where on a discrete lattice $\Delta x = \Delta t = 1$. The sound speed c_s is specific to the lattice structure (again refer to Appendix A).

Following Shan *et al.* [8], the systematic procedure to derive higher-order LB models by expansion of Hermite

polynomials, the third-order expansion, yields

$$f_\alpha^{\mathrm{eq},\phi} = w_\alpha \rho^\phi \left\{ 1 + \underbrace{\frac{\boldsymbol{\xi}_\alpha \cdot \boldsymbol{u}^m}{c_s^2}}_{\text{1st order}} + \underbrace{\frac{1}{2}\left[\frac{(\boldsymbol{\xi}_\alpha \cdot \boldsymbol{u}^m)^2}{c_s^4} - \frac{(u^m)^2}{c_s^2} \right]}_{\text{2nd order}} \right.$$
$$\left. + \underbrace{\frac{1}{6}\frac{\boldsymbol{\xi}_\alpha \cdot \boldsymbol{u}^m}{c_s^2}\left[\frac{(\boldsymbol{\xi}_\alpha \cdot \boldsymbol{u}^m)^2}{c_s^4} - \frac{3(u^m)^2}{c_s^2} \right]}_{\text{3rd order}} \right\}, \quad (6)$$

where w_α are the lattice weights and $\boldsymbol{u}^m \cdot \boldsymbol{u}^m = (u^m)^2$. The density ρ^ϕ at each lattice site in space $\boldsymbol{x}$ is defined by summation of the distribution f_α^ϕ (zeroth-order moment). Momentum is then computed by the sum of $f_\alpha^\phi \boldsymbol{\xi}_\alpha$ (first-order moment) and a shift in momentum due to the additional force contribution

$$\rho^\phi = \sum_\alpha f_\alpha^\phi, \quad (7\mathrm{a})$$

$$\rho^\phi \boldsymbol{u}^\phi = \sum_\alpha f_\alpha^\phi \boldsymbol{\xi}_\alpha + \frac{\Delta t}{2} \boldsymbol{F}^\phi. \quad (7\mathrm{b})$$

To satisfy the total momentum conversation, instead of $\boldsymbol{u}^\phi$ the variable $\boldsymbol{u}^m$ is used in $f_\alpha^{\mathrm{eq},\phi}$ [Eq. (6)], which is generally referred to as the common mixture velocity [39], and is evaluated by

$$\boldsymbol{u}^m = \frac{\sum_\phi^{\mathcal{S}} \rho^\phi \boldsymbol{u}^\phi \cdot \omega^\phi}{\sum_\phi^{\mathcal{S}} \rho^\phi \cdot \omega^\phi}. \quad (8)$$

The total velocity of the fluid mixture (barycentric velocity) takes the form of $\boldsymbol{u} = \frac{\sum_\phi^{\mathcal{S}} \rho^\phi \boldsymbol{u}^\phi}{\sum_\phi^{\mathcal{S}} \rho^\phi}$. More details regarding this interpretation of this force contribution in the collision, known as the explicit forcing model, and mixture velocity have already been covered extensively in a recent paper by Küllmer *et al.* [40].

The total momentum flux tensor [30]

$$P_{ij}^{\mathrm{tot}} = P_{ij}^{\mathrm{kin}} + P_{ij}^{\mathrm{int}} \quad (9)$$

involves contributions from a kinetic part P_{ij}^{kin} obtained directly from the lattice distribution (second-order moment) and additional contributions due to nonideal interactions from the SC pseudopotential model. Close to equilibrium, the kinetic part of Eq. (9) can be approximated directly from distributions [30,36]

$$P_{ij}^{\mathrm{kin}} = \rho c_s^2 \delta_{ij} + \rho u_i^m u_j^m \approx \sum_\phi^{\mathcal{S}} \sum_\alpha f_\alpha^{\mathrm{eq},\phi} \xi_{\alpha,i} \xi_{\alpha,j}, \quad (10)$$

where δ_{ij} is the Kronecker delta and $\rho = \sum_\phi^{\mathcal{S}} \rho^\phi$. The term ρc_s^2 in Eq. (10) is identified as the ideal contribution and the following term can be defined in relation to $\boldsymbol{u}^m$, since at equilibrium the component-specific velocity $\boldsymbol{u}^\phi$ converges towards the mixture velocity $\boldsymbol{u}^m$. Note that, for typographical convenience, here and throughout this work, we denote the ith and jth components of tensors (of any rank) by subscripts. The discrete lattice velocity $\boldsymbol{\xi}_\alpha$ (rank-1 tensor), due to dependence on α, is, for example, the ith component, denoted by $\xi_{\alpha,i}$.

In the total momentum flux tensor (9) the kinetic part, as defined in Eq. (10), is an approximation and may in addition involve higher-order contributions as discussed in [30,41,42]. Nevertheless, central to the analysis in this work is the interaction pressure tensor P_{ij}^{int} part of Eq. (9).

III. NONIDEAL INTERACTIONS

The ith component of the force at $\boldsymbol{x}$ due to intra- and interparticle interactions in the pseudopotential SC multicomponent model [13] can be defined by

$$
\begin{aligned}
F_i^{\phi}(\boldsymbol{x}) = - & \left[\psi^{\phi}(\boldsymbol{x}) \mathcal{G}^{\phi\phi} \sum_{\alpha} \tilde{w}_{\alpha}(|\boldsymbol{e}_{\alpha}|^2) \psi^{\phi}(\boldsymbol{x}+\boldsymbol{e}_{\alpha}) e_{\alpha,i} \right. \\
& \left. + \Psi^{\phi}(\boldsymbol{x}) \sum_{\varphi\neq\phi}^{\mathcal{S}} \mathcal{G}^{\phi\varphi} \sum_{\alpha} \tilde{w}_{\alpha}(|\boldsymbol{e}_{\alpha}|^2) \Psi^{\varphi}(\boldsymbol{x}+\boldsymbol{e}_{\alpha}) e_{\alpha,i} \right],
\end{aligned}
$$
(11)

where $\mathcal{G}$ is the interaction strength between components whose negative (positive) sign defines attraction (repulsion), which is essentially used as a control variable to achieve various transport properties. Component-specific pseudopotentials for intra-interaction (self-interaction) $\psi(\rho)$ and inter-interactions (cross-interactions) $\Psi(\rho)$ can take various forms depending on the type of application [23,30]. For example, a popular choice would be [23,30,33] $\psi^{\phi} = \rho^0[1 - e^{-\rho^{\phi}/\rho^0}]$ and $\Psi^{\phi} = \rho^{\phi}$, where ρ^0 is a constant used to refine the interface resolution [43]. It is interesting to note that $\sum_{\alpha} \tilde{w}_{\alpha}\psi(\boldsymbol{x}+\boldsymbol{\xi}_{\alpha})\boldsymbol{\xi}_{\alpha}$ is effectively the gradient [44], that is, essentially $\boldsymbol{F} \propto -\psi\mathcal{G}\nabla\psi$. From this point of view, it is clear that the intra- and intermolecular interactions only exist in the bulk phase in the presence of gradients $\nabla\rho$ and when dissimilar components coexist in the same space $\boldsymbol{x} \pm \boldsymbol{\xi}$ (e.g., fluid mixtures and phase interface), respectively.

An important feature of the interaction force (11) is that it is directly applicable on any lattice structure. The term $\tilde{w}_{\alpha}(|\boldsymbol{e}_{\alpha}|^2)$ represents weights for the force interaction links $\boldsymbol{e}_{\alpha}$ in Eq. (11) and does *not* strictly have to be the same as the discrete velocity weights $w_{\alpha}(\boldsymbol{\xi}_{\alpha})$. This has traditionally allowed the force interaction to be at a specific isotropy order independent of the lattice structure (see [43]). This is useful for low-isotropy-order lattice structures, such as the popular D2Q9, which are plagued by spurious currents. The lattice structure in Fig. 1, and high-order lattice models in general, have algebraic accuracy of isotropy order of 6 or greater. [This holds for any lattice model that can completely recover the third-order equilibrium distribution function (6). The lattice model with the shortest lattice structure to comply with this is the D2Q17 model [8].] This will give confidence that spurious currents are minimized. As such, when using high-order lattice structures, there may not be any need for a specific force interaction model, such as the eighth-order-isotropy force interaction model in [32], and instead the lattice structure is used directly to model interactions. For this reason, hereinafter, we omit $\boldsymbol{e}_{\alpha}$ and use the lattice velocities $\boldsymbol{\xi}_{\alpha}$ to also define interaction vectors, and in addition treat $\tilde{w}_{\alpha}(|\boldsymbol{\xi}_{\alpha}|^2) \propto w_{\alpha}(|\boldsymbol{\xi}_{\alpha}|^2)$. Furthermore, it is convenient to ensure certain conditions on the mth-order isotropy coefficient $\mathcal{C}_m$. Here we ensure that the second-order isotropy coefficient

is normalized to unity $\mathcal{C}_2 = \delta_{ij} = 1$, which is achieved by rescaling weights by $\tilde{w}_{\alpha} = w_{\alpha}/c_s^2$ (details regarding isotropy are provided in Appendix B). As a result, the fourth-order isotropy coefficient $\mathcal{C}_4$ is now equal to c_s^2 on any lattice structure. This allows $\mathcal{C}_2$ to remain constant and $\mathcal{C}_4$ to always be equal to the sound speed squared for any high-order lattice structure.

A. On-lattice interaction pressure tensor

Here we detail the consequent interaction pressure tensor, at the discrete level, from the nonideal interaction forces (11) applied directly on high-order lattices. To be consistent with the exact lattice theory, we follow Shan [32] and derive a generalized form that can be used on a variety of high-order lattices. As mentioned earlier, contributions vary depending on the lattice and as such we consider the contributions from the symmetry group individually. Symmetry groups (z) are uniquely identified by the square length of the vectors $z = |\boldsymbol{\xi}_1|^2, |\boldsymbol{\xi}_2|^2, \ldots, |\boldsymbol{\xi}_{\alpha}|^2$. Here and throughout this work, we denote by superscripts variables that are classified to comply with, or be dependent on, specific symmetry groups, e.g., $\boldsymbol{\xi}_{\alpha}^{z=2}$ or equivalently $\boldsymbol{\xi}_{\alpha}^z \forall z = 2$. The total interaction pressure tensor P_{ij}^{int} is then the sum of all $\mathcal{P}_{ij}^{\text{int}(z)}$ contributions

$$
P_{ij}^{\text{int}} = \sum_{\phi}^{\mathcal{S}} \sum_{z} \mathcal{P}_{ij}^{\phi,\text{int}(z)}.
$$
(12)

Obviously, the smallest symmetry groups ($z \leqslant 2$) are the simplest and are therefore used here as a starting point. We classify this as a unique subgroup which we denote by $\tilde{z}$, $\tilde{z} := z \forall z \leqslant 2$. For typographical convenience, we use ψ to denote any form of pseudopotential and omit explicit fluid-component ϕ dependence.

We now follow on directly from the brief introduction in Sec. I and provide a overview of the key concepts of exact lattice theory (for more details refer to [32]). The objective of the exact lattice theory is to link the force with the pressure tensor at the discrete level, which compels the principles of Eq. (1) to be satisfied, that is, to define the momentum flux tensor of interactions through an infinitesimal area element $d\mathbf{A}$ in space $\boldsymbol{x}$. This by definition requires $P_{ij}^{\text{int}} d\mathbf{A}_j$ to be the ith component of the sum of all interaction pairs (sum of all interaction force vectors $\boldsymbol{F}$) through $d\mathbf{A}$, i.e., $-\sum_i F_i = \sum_{i,j} P_{ij}^{\text{int}} d\mathbf{A}_j$. On a discrete lattice, the interpretation of this concept is simplified by considering a horizontal $d\mathbf{A}^{(x)}$ and a vertical $d\mathbf{A}^{(y)}$ unit area element along the principle axis of the lattice at $\boldsymbol{x}$. The pressure tensor at $\boldsymbol{x}$ is then defined by all possible force vectors passing through $d\mathbf{A}^{(x)}$ and $d\mathbf{A}^{(y)}$. The ith component of the total force through $d\mathbf{A}^{(j)}$ is then $-\sum_i F_i = \sum_{i,j} P_{ij}^{\text{int}} d\mathbf{A}_j^{(j)}$. See, for example, Fig. 2(a), where the contribution from the force vectors along $\boldsymbol{\xi}_{25}$ through $d\mathbf{A}^{(x)}$ is clearly equal to $-\sum_y F_y = \sum_{i,x} \mathcal{P}_{ix}^{\text{int}} d\mathbf{A}_x^{(x)} = 0$. (Note that the illustrations in Fig. 2 are elaborated upon later in this section.) A key observation made in [32] is that along any single $\boldsymbol{\xi}_{\alpha}$ the number of interaction force vectors passing through a unit area element at any lattice site $\boldsymbol{x}$ is exactly equal to the components of the interaction vector $\boldsymbol{\xi}_{\alpha}$, namely, the number of force vectors through $d\mathbf{A}^{(x)}$ is $\xi_{\alpha,y}$ and through $d\mathbf{A}^{(y)}$ is $\xi_{\alpha,x}$.
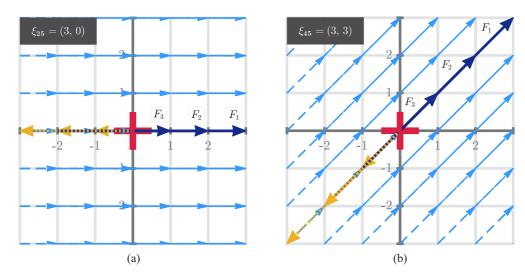
FIG. 2. Illustration of the force vectors along the vectors $\boldsymbol{\xi}_\alpha$ that belong to symmetry group $\bar{z}$ and pass through (bold solid arrows) the infinitesimal horizontal $d\mathbf{A}^{(x)}$ and vertical $d\mathbf{A}^{(y)}$ unit area elements (bold red line) centered at $\boldsymbol{x}$. In reference to the Q49ZOTT lattice in Fig. 1, force vectors along (a) $\boldsymbol{\xi}_{25}$ ($\bar{z}=9$) and (b) $\boldsymbol{\xi}_{45}$ ($\bar{z}=18$) are shown. In both (a) and (b), there is a total of six ($2\mathcal{E}^z$) force vectors contributing equally to their respective interaction pressure tensor, i.e., $\mathcal{P}_{ij}^{\mathrm{int},\bar{z}=9}$ and $\mathcal{P}_{ij}^{\mathrm{int},\bar{z}=18}$. The six force vectors consist of four different classes of vectors; one ($\boldsymbol{F}_1$) starts and another ends (accounted for along the opposite $\boldsymbol{\xi}_a$) at $\boldsymbol{x}$ and two ($\boldsymbol{F}_2$ and $\boldsymbol{F}_3$) pass through $\boldsymbol{x}$. Labeled force vectors are those to be explicitly considered along each respective $\boldsymbol{\xi}_\alpha$. The unlabeled bold dotted arrows are not considered along vectors $\boldsymbol{\xi}_\alpha$ but are instead accounted for along the opposite $\boldsymbol{\xi}_a$ (hence the direction of arrows) as a result of symmetry and summation around the lattice, for example, in this case (a) $\boldsymbol{\xi}_{27}$ and (b) $\boldsymbol{\xi}_{47}$. These are automatically considered in Eq. (15).

According to [32], if we consider the case where along $\boldsymbol{\xi}_\alpha$ all forces passing through any unit area element are of equal magnitude, then, from the above analysis, the pressure tensor is defined by multiplying this magnitude by $\boldsymbol{\xi}_\alpha\boldsymbol{\xi}_\alpha$.[1]

Since it cannot be guaranteed that over the whole force field all magnitudes are the same, the *average* of total forces through the unit area elements is taken instead [32,45]. Using nearest neighbors ($\tilde{z}$, where the interaction range $|\boldsymbol{\xi}_\alpha^{\tilde{z}}| \leqslant 1$) to illustrate this, as done in [32,34], we consider all possible forces along a class of vector, in this case $\boldsymbol{\xi}_l$, through any unit area element centered at $\boldsymbol{x}$.

Since only nearest neighbors are considered, we find that over the entire lattice at $\boldsymbol{x}$ there is a total of two interaction pairs (force vectors) through $d\mathbf{A}^{(x)}$ or $d\mathbf{A}^{(y)}$, or both, i.e., one in which a particle at $\boldsymbol{x}$ interacts with a particle at $\boldsymbol{x}+\boldsymbol{\xi}_l$ and a second where a particle at $\boldsymbol{x}-\boldsymbol{\xi}_l$ interacts with the particle at $\boldsymbol{x}$. As a result, the averaged pseudopotential interaction force magnitude is then defined by (the use of $\boldsymbol{\xi}_l := \boldsymbol{\xi}_\alpha^{\tilde{z}}$ is strictly only for the example here)

$$-\mathcal{G}\tilde{w}_l\psi(\boldsymbol{x})\frac{\psi(\boldsymbol{x}+\boldsymbol{\xi}_l)+\psi(\boldsymbol{x}-\boldsymbol{\xi}_l)}{2},$$

where the contribution to the interaction pressure tensor is then

$$\mathcal{G}\left[\tilde{w}_l\psi(\boldsymbol{x})\frac{\psi(\boldsymbol{x}+\boldsymbol{\xi}_l)+\psi(\boldsymbol{x}-\boldsymbol{\xi}_l)}{2}\xi_{l,i}\xi_{l,j}\right].$$

----

[1]It should be noted that Sbragaglia and Belardinelli [34] demonstrated this link between the force and pressure tensor from a statistical mechanics point of view, following the theory of Irving and Kirkwood [45], adopted on the lattice for $z \leqslant 2$.

We identify that the terms within the square brackets can be represented by the sum of all α on the lattice divided by 2, $\frac{1}{2}\psi(\boldsymbol{x})\sum_\alpha \tilde{w}_\alpha\psi(\boldsymbol{x}+\boldsymbol{\xi}_\alpha)\xi_{\alpha,i}\xi_{\alpha,j}$, which is possible due to the symmetry of the lattice structure (e.g., $\boldsymbol{\xi}_5 = -\boldsymbol{\xi}_7$ in Fig. 1). Rearranging according to this, it is possible to rewrite the above, in terms of the *total* interaction pressure tensor at $\boldsymbol{x}$ (all contributions along all $\boldsymbol{\xi}_l$ on the lattice $\boldsymbol{\xi}_\alpha^z \ \forall z = \tilde{z}$),

$$\mathcal{P}_{ij,}^{\mathrm{int}(\tilde{z})}(\boldsymbol{x}) = \frac{1}{2}\mathcal{G}\psi(\boldsymbol{x})\sum_\alpha \tilde{w}_\alpha\psi\left(\boldsymbol{x}+\boldsymbol{\xi}_\alpha^{\tilde{z}}\right)\xi_{\alpha,i}^{\tilde{z}}\xi_{\alpha,j}^{\tilde{z}}. \qquad (13)$$

It is then straightforward to extend this relation to consider both the intra- and inter-interaction, i.e., in a fluid mixture of $\mathcal{S}$ components, where Eq. (13) for component ϕ would be expressed by

$$\mathcal{P}_{ij,}^{\phi,\mathrm{int}(\tilde{z})}(\boldsymbol{x}) = \frac{1}{2}\bigg[\psi^\phi(\boldsymbol{x})\mathcal{G}^{\phi\phi}\sum_\alpha \tilde{w}_\alpha\psi^\phi\left(\boldsymbol{x}+\boldsymbol{\xi}_\alpha^{\tilde{z}}\right)\xi_{\alpha,i}^{\tilde{z}}\xi_{\alpha,j}^{\tilde{z}}$$
$$+ \ \Psi^\phi(\boldsymbol{x})\sum_{\varphi\neq\phi}^{\mathcal{S}}\mathcal{G}^{\phi\varphi}\sum_\alpha \tilde{w}_\alpha\Psi^\varphi\left(\boldsymbol{x}+\boldsymbol{\xi}_\alpha^{\tilde{z}}\right)\xi_{\alpha,i}^{\tilde{z}}\xi_{\alpha,j}^{\tilde{z}}\bigg]. \qquad (14)$$

Equations (14) and (13) for the case of a single fluid system are the exact discrete definition of P_{ij}^{int} (12) for a standard lattice, such as Q9, which satisfies Eq. (1). However, on higher-order lattices, where the interaction range spans multiple lattice sites ($\xi_{\alpha,i}, \xi_{\alpha,j} > 1$), there are various additional force vectors contributing to P_{ij}^{int} [Eq. (12)] that are not captured by Eq. (13).

In order to account for all contributions on any arbitrary high-order lattice and satisfy Eq. (1), we expand upon the concept detailed above. First, due to symmetry and the
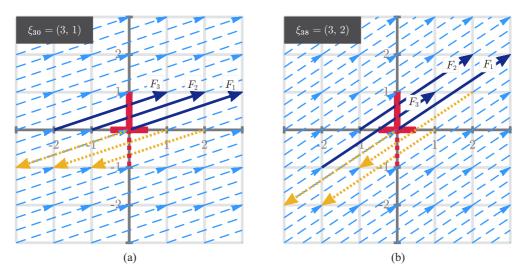
FIG. 3. Illustration of the force vectors along the vectors $\boldsymbol{\xi}_\alpha$ (of the Q49ZOTT lattice in Fig. 1) that belong to symmetry group $\hat{z}$ and pass through (bold solid arrows) the vertical infinitesimal $d\mathbf{A}^{(y)}$ unit area element (red bold solid line). The unlabeled bold dotted arrows which pass through the red bold dotted line ($d\mathbf{A}^{(y)}$) are accounted for along $\boldsymbol{\xi}_a$. In both (a) and (b), it is clear that considering contributions to $d\mathbf{A}^{(y)}$ in turn correctly accounts for those passing through the horizontal infinitesimal $d\mathbf{A}^{(x)}$ unit area element (red bold solid line) centered at $\boldsymbol{x}$. (a) For vector $\boldsymbol{\xi}_{30}$ there are six ($2\mathcal{E}^z$) force vectors with equal contribution to $\mathcal{P}_{ij}^{\mathrm{int},\hat{z}=10}$. (b) For vector $\boldsymbol{\xi}_{38}$ there are also six force vectors, however, they do not contribute equally to $\mathcal{P}_{ij}^{\mathrm{int},\hat{z}=13}$. The contributions to $\hat{z}=10$ are automatically considered in Eq. (16), whereas those in $\hat{z}=13$ can still be obtained with Eq. (16) but require a unique condition (C_β) to correct the different contributions of $\boldsymbol{F}_2$ and $\boldsymbol{F}_3$ (see the text).

summation $\sum_\alpha$ around the lattice, we only need to consider half the total number of force vectors, that is, only those along any single $\boldsymbol{\xi}_\alpha$, as done in Eq. (13). To satisfy these conditions, the basic general rule is that force vectors along any given vector $\boldsymbol{\xi}_\alpha^z \,\forall z > 2$ contribute to the pressure tensor if they pass through the horizontal $d\mathbf{A}^{(x)}$ or the vertical $d\mathbf{A}^{(y)}$, or both, unit area elements centered at $\boldsymbol{x}$, which includes if these start at, or pass through, the center of $\boldsymbol{x}$. In Figs. 2 and 3 we illustrate contributions accounted for along each respective $\boldsymbol{\xi}_\alpha$ (which make up half of the total contribution) by bold solid arrows and those accounted for along their opposite $\boldsymbol{\xi}_a$ (the other half) by bold dotted arrows. Hereinafter we denote the opposite of any $\boldsymbol{\xi}_\alpha$ by $\boldsymbol{\xi}_a$. Moreover, we consider $\mathcal{P}_{ij}^{\mathrm{int}(z)} \,\forall z > 2$ in two subgroups, which we denote by $\bar{z}$ and $\hat{z}$, illustrated in Figs. 2 and 3, respectively. Again we recall the use of superscript $\bar{z}$ or $\hat{z}$ to denote variables that are classified to comply with these subgroups, i.e., $\boldsymbol{\xi}_\alpha^{\bar{z}}$ or equivalently $\boldsymbol{\xi}_\alpha^z \,\forall z = \bar{z}$. In the following, the Q49ZOTT lattice illustrated in Fig. 1 will be used as an example (a single lattice structure for the sake of convenience). Reasons for this particular lattice will be elaborated upon later.

The first subgroup, which we classify by $\bar{z}$, considers all vectors that are purely axial, $\xi_{\alpha,i} \cdot \xi_{\alpha,j} = 0$, $i \neq j$, or purely diagonal with components of equal lengths, $\xi_{\alpha,i} = \xi_{\alpha,j}$. Two examples of vectors belonging to this first group, $\boldsymbol{\xi}_{25}$ ($\bar{z} = 9$) and $\boldsymbol{\xi}_{45}$ ($\bar{z} = 18$), are illustrated in Fig. 2, where in both cases there is a total of six force vectors that consist of four different classes of vectors (more details in Fig. 2). It can be clearly seen that along $\boldsymbol{\xi}_{25}$ there are three (equal to $\xi_{25,x}$) force vectors through $d\mathbf{A}^{(y)}$ and zero through $d\mathbf{A}^{(x)}$ (equal to $\xi_{25,y}$), consistent with analysis in [32]. Along $\boldsymbol{\xi}_{45}$ there is a total of three (equal to $\xi_{45,x}$ and $\xi_{45,y}$) force vectors through both $d\mathbf{A}^{(x)}$ and $d\mathbf{A}^{(y)}$. For this reason, in both cases, all six force

vectors contribute equally to the interaction pressure tensor. First, to account for $\boldsymbol{F}_1$, along any $\boldsymbol{\xi}_\alpha^{\bar{z}}$, the same definition from Eq. (13) can be used and this is true for any z group. In what follows we therefore focus on obtaining the additional contributions that appear when $z > 2$ (e.g., $\boldsymbol{F}_2$ and $\boldsymbol{F}_3$). We identify that the number of additional contributions is defined by $\mathcal{E}^z - 1$, where the scalar variable $\mathcal{E}^z$ is the largest of the absolute value of the components in the vector $\boldsymbol{\xi}_\alpha$ of the symmetry group z: $\mathcal{E}^z = \max_\alpha(|\boldsymbol{\xi}_\alpha^z|) \,\forall \alpha \in \boldsymbol{\xi}_\alpha^z$. For example, consider the $\boldsymbol{\xi}_{11}$ vector of Q49ZOTT where $z = 9$ (see Fig. 1): $\mathcal{E}^9 = \max_\alpha(|\boldsymbol{\xi}_{11}^{z=9}|) = 3 \,\forall \alpha \in \boldsymbol{\xi}_\alpha^{z=9}$. The total number of force vectors, those along $\boldsymbol{\xi}_\alpha$ and $\boldsymbol{\xi}_a$ (all bold arrows in Fig. 2), can then be defined by $2\mathcal{E}^z$ and with this the total average can be achieved by multiplying all force vectors by $1/2\mathcal{E}^z$. Furthermore, in Fig. 2 it can be noticed that additional contributions $\boldsymbol{F}_2$ and $\boldsymbol{F}_3$ are simply vectors shifted along the unit vector[2] $\mathbf{U}_\alpha$ along each respective $\boldsymbol{\xi}_\alpha^z$. Clearly, the total number of shifts is equal to the total number of additional contributions, i.e., $\mathcal{E}^z - 1$. It is convenient to view this in terms of summation, where we have some starting vector (e.g., $\boldsymbol{F}_3$ in Fig. 2) and then shift progressively in the direction of $\mathbf{U}_\alpha$ up to some final vector (e.g., $\boldsymbol{F}_2$ in Fig. 2). This final vector is always defined as the additional contribution that resides closest to $\boldsymbol{F}_1$ and is found by shifting by one unit backward (opposite the direction of $\mathbf{U}_\alpha$), that is, a vector that starts at $\boldsymbol{x} - \boldsymbol{\xi}_\alpha + \mathbf{N}$

---

[2]The directional unit vector $\mathbf{U}_\alpha$ of $\boldsymbol{\xi}_\alpha$ is defined by $\mathbf{U}_\alpha(\boldsymbol{\xi}_\alpha) = \mathbf{U} \circ \mathrm{sgn}(\boldsymbol{\xi}_\alpha)$, where $\circ$ is the Hadamard product, $\mathbf{U}$ is a vector of 1's, i.e., $\mathbf{U} = (1, 1)$, and the notation sgn denotes the signum function, which returns the sign of each element of the input vector, e.g., $\mathrm{sgn}(-3, 3) = (-1, 1)$.

and extends to (ends at) $x + \mathbf{N}$, where $\mathbf{N}(\boldsymbol{\xi}_\alpha) = (\mathcal{E}^z - 1)\mathbf{U}_\alpha$. The starting vector, say, $\boldsymbol{F}_0$, is of course the vector located farthest away from $\boldsymbol{F}_1$ (e.g. $\boldsymbol{F}_3$ in Fig. 2), where in addition to this we consider that such a vector cannot end (the tip of the arrow) at the center x nor shift farther away from the center x (with respect to $\mathbf{U}_\alpha$). For this reason, $\boldsymbol{F}_0$ will end (the tip of the arrow) on one of the neighboring or nearest-neighboring nodes (see, e.g., the $\boldsymbol{F}_3$ in both Fig. 2 and 3). Fortunately, this is simply equal to the directional unit vector $\mathbf{U}_\alpha$ of each $\boldsymbol{\xi}_\alpha^{\bar{z}}$. Considering this, $\boldsymbol{F}_0$ can then be defined as a vector that starts at $x - \boldsymbol{\xi}_\alpha + \boldsymbol{\varepsilon}_{\beta=1}$ and extends to (ends at) $x + \boldsymbol{\varepsilon}_{\beta=1}$, where we set initially $\boldsymbol{\varepsilon}_{\beta=1} = \mathbf{U}_\alpha$. This vector $\boldsymbol{\varepsilon}_\beta^{\bar{z}}$ then progressively shifts along $\mathbf{N}^{\bar{z}}$ until $\boldsymbol{\varepsilon}_\beta^{\bar{z}} = \mathbf{N}^{\bar{z}}$ and as such we can define $\boldsymbol{\varepsilon}_\beta^{\bar{z}} : \beta = 1, \ldots, (\mathcal{E}^z - 1)$.

Considering the above, we can express this $\bar{z}$-group interaction pressure tensor in the form

$$\mathcal{P}_{ij}^{\mathrm{int},(\bar{z})}(\boldsymbol{x}) = \psi(\boldsymbol{x})\mathcal{G}\sum_\alpha \frac{\tilde{w}_\alpha}{2\mathcal{E}^{\bar{z}}}\psi(\boldsymbol{x}+\boldsymbol{\xi}_\alpha^{\bar{z}})\xi_{\alpha,i}^{\bar{z}}\xi_{\alpha,j}^{\bar{z}} + \sum_\alpha \sum_\beta^{\boldsymbol{\varepsilon}_\beta^{\bar{z}}=\mathbf{N}^{\bar{z}}} \frac{\tilde{w}_\alpha}{2\mathcal{E}^{\bar{z}}}\big[\mathcal{G}\psi(\boldsymbol{x}+\boldsymbol{\varepsilon}_\beta^{\bar{z}})\cdot\psi(\boldsymbol{x}-\boldsymbol{\xi}_\alpha^{\bar{z}}+\boldsymbol{\varepsilon}_\beta^{\bar{z}})\xi_{\alpha,i}^{\bar{z}}\xi_{\alpha,j}^{\bar{z}}\big], \tag{15}$$

where the first term on the right-hand side is essentially Eq. (13) and the summation over β, from the initial vector $\boldsymbol{\varepsilon}_\beta^{\bar{z}}$ up to the vector $\mathbf{N}^{\bar{z}}$, allows all other contributions of any unit area element to be considered for any $\boldsymbol{\xi}_\alpha^{\bar{z}}$. Here the sum over α implies $\sum_\alpha \boldsymbol{\xi}_\alpha = \sum_z \sum_\alpha \boldsymbol{\xi}_\alpha^z$, where in direct reference to Q49ZOTT in Fig. 1 this summation defines $\sum_\alpha \boldsymbol{\xi}_\alpha^{\bar{z}} = \sum_\alpha \boldsymbol{\xi}_\alpha$ for $\alpha = 9, \ldots, 12, 21, \ldots, 28, 45, \ldots, 48$.

The second subgroup, classified as $\hat{z}$, consists of diagonal vectors with mixed components $\xi_{\alpha,i} \neq \xi_{\alpha,j}$ and $\xi_{\alpha,i}, \xi_{\alpha,j} \neq 0$. In this $\hat{z}$ group, consider the two examples illustrated in Fig. 3, where we can see that there is a total of six $(2\mathcal{E}^z)$ force vectors contributing to the pressure tensor that consist of six different classes of vectors. It turns out that both $d\mathbf{A}^{(x)}$ and $d\mathbf{A}^{(y)}$ being centered at x does *not* allow contributions from $\boldsymbol{F}_3$ [in Fig. 3(a)] and $\boldsymbol{F}_2$ [in Fig. 3(b)] to be identified. To correctly account for these contributions on the lattice we can instead rely on the idea that if we consider only the unit area element for which the greatest number of force vectors pass through (e.g., the vertical $d\mathbf{A}^{(y)}$ in Fig. 3), then force vectors passing through its orthogonal unit area element (e.g., in this case the horizontal $d\mathbf{A}^{(x)}$) will also be accounted for. To demonstrate this, we first recall that from previous analysis along any $\boldsymbol{\xi}_\alpha$ the number of force vectors through $d\mathbf{A}^{(i)}$ and $d\mathbf{A}^{(j)}$ is equal to $\xi_{\alpha,j}$ and $\xi_{\alpha,i}$, respectively. If $|\xi_{\alpha,i}| = \mathcal{E}^{\hat{z}}$, then $d\mathbf{A}^{(j)}$ shifts from the center to now start at $x = (0, 0)$ and end at $x_j = U_{\alpha,i}$ (where $\mathbf{U}_{\alpha,i}$ is the directional unit vector of $\boldsymbol{\xi}_\alpha$). For example, as illustrated in Fig. 3, to consider contributions along $\boldsymbol{\xi}_\alpha$, the vector $d\mathbf{A}^{(y)}$ is shifted upward (red bold solid line) and along its opposite $\boldsymbol{\xi}_a$, the vector $d\mathbf{A}^{(y)}$ is shifted downward (red bold dotted line). As we can see in Fig. 3, by doing so, along $\boldsymbol{\xi}_{30}$, three force vectors ($\boldsymbol{F}_1$, $\boldsymbol{F}_2$, and $\boldsymbol{F}_3$) pass through $d\mathbf{A}^{(y)}$ and only one ($\boldsymbol{F}_1$) passes through $d\mathbf{A}^{(x)}$. Along $\boldsymbol{\xi}_{38}$, three force vectors ($\boldsymbol{F}_1$, $\boldsymbol{F}_2$, and $\boldsymbol{F}_3$) pass through $d\mathbf{A}^{(y)}$ and two ($\boldsymbol{F}_1$ and $\boldsymbol{F}_3$) pass through $d\mathbf{A}^{(x)}$. This is consistent with previous analysis [32] and the same can be done for the $\bar{z}$ group where the same equation (15) will be obtained. Visually, from Fig. 3, contributions for $\hat{z}$ appear more complex; however, the same principles used to obtain Eq. (15) apply here with some additional conditions.

First, similar to the $\bar{z}$ group, in this $\hat{z}$ group the same definition from Eq. (13) can be used to account for $\boldsymbol{F}_1$ for any $\boldsymbol{\xi}_\alpha^{\hat{z}}$. A condition is required on how vectors are shifted during the sum over β: Any ith component (where $i := x, y$) in vector $\boldsymbol{\varepsilon}_\beta$ at $\beta > 1$ is shifted (with respect to $U_{\alpha,i}$) provided $\varepsilon_{\beta-1,i} \neq \xi_{\alpha,i}^{\hat{z}}$; otherwise the ith component at $\beta > 1$ remains as it is, i.e., $\varepsilon_{\beta,i} = \varepsilon_{\beta-1,i}$. This can be clearly seen in Fig. 3(a), where $\boldsymbol{F}_3$ (at $\beta = 1$), with $\varepsilon_{1,y} - \xi_{30,y} = 0$, and $\boldsymbol{F}_2$ (at $\beta = 2$) are not shifted vertically and $\varepsilon_{2,y} = \varepsilon_{1,y}$. There is also one unique condition around the additional contribution on vectors $\boldsymbol{\xi}_\alpha^{\hat{z}=13}$, such as $\boldsymbol{\xi}_{38}$ in Fig. 3(b). As we have identified previously, $\boldsymbol{F}_3$ passes through both $d\mathbf{A}^{(x)}$ and $d\mathbf{A}^{(y)}$ whereas $\boldsymbol{F}_2$ passes through only $d\mathbf{A}^{(y)}$ and therefore they do not contribute equally to $\mathcal{P}_{ij}^{\mathrm{int},\hat{z}=13}$. To account for this unequal contribution we rescale these contributions but ensure that the overall average along $\boldsymbol{\xi}_\alpha^{\hat{z}=13}$ will correctly reduce to $\frac{1}{2}$. We assume that $\boldsymbol{F}_1$ retains its contribution, i.e., $1/2\mathcal{E}^z$. Since $\boldsymbol{F}_3$ passes through both area elements we assume that its contribution is $\mathcal{E}^z/(\mathcal{E}^z - 1) = \frac{3}{2}$ greater than $\boldsymbol{F}_1$, and the contribution from $\boldsymbol{F}_2$ is half of $\boldsymbol{F}_1$ since $(\mathcal{E}^z - 1) - \frac{3}{2} = \frac{1}{2}$.

This $\hat{z}$-group interaction pressure tensor can be expressed in the form

$$\mathcal{P}_{ij}^{\mathrm{int}(\hat{z})}(\boldsymbol{x}) = \psi(\boldsymbol{x})\mathcal{G}\sum_\alpha \frac{\tilde{w}_\alpha}{2\mathcal{E}^{\hat{z}}}\psi(\boldsymbol{x}+\boldsymbol{\xi}_\alpha^{\hat{z}})\xi_{\alpha,i}^{\hat{z}}\xi_{\alpha,j}^{\hat{z}} + \sum_\alpha \sum_\beta^{\boldsymbol{\varepsilon}_\beta^{\hat{z}}=\mathbf{N}^{\hat{z}}} C_\beta \frac{\tilde{w}_\alpha}{2\mathcal{E}^{\hat{z}}}\big[\mathcal{G}\psi(\boldsymbol{x}+\boldsymbol{\varepsilon}_\beta^{\hat{z}})\cdot\psi(\boldsymbol{x}-\boldsymbol{\xi}_\alpha^{\hat{z}}+\boldsymbol{\varepsilon}_\beta^{\hat{z}})\xi_{\alpha,i}^{\hat{z}}\xi_{\alpha,j}^{\hat{z}}\big], \tag{16}$$

where we introduce an additional constant C_β in the second term to account for the variation in contributions. The modified factor C_β is required *only* for $\hat{z} = 13$, where during the sum over β, the additional contribution, this factor is initially set to $C_{\beta=1} = \frac{3}{2}$ and then $C_{\beta=(3-1)} = \frac{1}{2}$. For any other symmetry group $\hat{z} < 13$ this factor is set to unit constant $C_\beta = 1$.

Finally, the full form of the general expression for the total interaction pressure tensor due to Eq. (11) including all nonideal interactions, as done in Eq. (14), is shown here as a single equation. We recall that in both Eqs. (15) and (16) the first term is

essentially Eq. (13), which allows us to define the total interaction pressure tensor (12) explicitly by

$$
\begin{aligned}
P_{ij}^{\mathrm{int}}(\boldsymbol{x}) = \sum_{\phi}^{\mathcal{S}} \sum_{z} \mathcal{P}_{ij}^{\phi,\mathrm{int}(z)}(\boldsymbol{x}) = \sum_{\phi}^{\mathcal{S}} & \left\{ \sum_{\alpha} \frac{\tilde{w}_{\alpha}}{2\mathcal{E}^z} \left(\mathcal{G}^{\phi\phi} \psi^{\phi}(\boldsymbol{x}) \cdot \psi^{\phi}(\boldsymbol{x}+\boldsymbol{\xi}_{\alpha}) \xi_{\alpha,i} \xi_{\alpha,j} + \Psi^{\phi}(\boldsymbol{x}) \sum_{\varphi \neq \phi}^{\mathcal{S}} \mathcal{G}^{\phi\varphi} \Psi^{\varphi}(\boldsymbol{x}+\boldsymbol{\xi}_{\alpha}) \xi_{\alpha,i} \xi_{\alpha,j} \right) \right. \\
& + \sum_{\alpha} \sum_{\beta}^{\boldsymbol{\varepsilon}_{\beta}^{\bar{z}}=\mathbf{N}^{\bar{z}}} \frac{\tilde{w}_{\alpha}}{2\mathcal{E}^{\bar{z}}} \left(\mathcal{G}^{\phi\phi} \psi^{\phi}(\boldsymbol{x}+\boldsymbol{\varepsilon}_{\beta}^{\bar{z}}) \cdot \psi^{\phi}(\boldsymbol{x}-\boldsymbol{\xi}_{\alpha}^{\bar{z}}+\boldsymbol{\varepsilon}_{\beta}^{\bar{z}}) \xi_{\alpha,i}^{\bar{z}} \xi_{\alpha,j}^{\bar{z}} + \sum_{\varphi \neq \phi}^{\mathcal{S}} \mathcal{G}^{\phi\varphi} \Psi^{\phi}(\boldsymbol{x}+\boldsymbol{\varepsilon}_{\beta}^{\bar{z}}) \cdot \Psi^{\varphi}(\boldsymbol{x}-\boldsymbol{\xi}_{\alpha}^{\bar{z}}+\boldsymbol{\varepsilon}_{\beta}^{\bar{z}}) \xi_{\alpha,i}^{\bar{z}} \xi_{\alpha,j}^{\bar{z}} \right) \\
& \left. + \sum_{\alpha} \sum_{\beta}^{\boldsymbol{\varepsilon}_{\beta}^{\hat{z}}=\mathbf{N}^{\hat{z}}} C_{\beta} \frac{\tilde{w}_{\alpha}}{2\mathcal{E}^{\hat{z}}} \left(\mathcal{G}^{\phi\phi} \psi^{\phi}(\boldsymbol{x}+\boldsymbol{\varepsilon}_{\beta}^{\hat{z}}) \cdot \psi^{\phi}(\boldsymbol{x}-\boldsymbol{\xi}_{\alpha}^{\hat{z}}+\boldsymbol{\varepsilon}_{\beta}^{\hat{z}}) \xi_{\alpha,i}^{\hat{z}} \xi_{\alpha,j}^{\hat{z}} + \sum_{\varphi \neq \phi}^{\mathcal{S}} \mathcal{G}^{\phi\varphi} \Psi^{\phi}(\boldsymbol{x}+\boldsymbol{\varepsilon}_{\beta}^{\hat{z}}) \cdot \Psi^{\varphi}(\boldsymbol{x}-\boldsymbol{\xi}_{\alpha}^{\hat{z}}+\boldsymbol{\varepsilon}_{\beta}^{\hat{z}}) \xi_{\alpha,i}^{\hat{z}} \xi_{\alpha,j}^{\hat{z}} \right) \right\}.
\end{aligned}
$$
(17)

It is noted that Eq. (15) can account for any $\bar{z}$ group of interactions due to summation over β. However, for $\hat{z}$ groups of mixed components larger than those shown in Fig. 3 (i.e., $\hat{z} > 13$), Eq. (16) is limited to vectors that have at least one component equal to one, e.g., $\boldsymbol{\xi}_{\alpha}^{\hat{z}=17} = (4, 1)$ and $\boldsymbol{\xi}_{\alpha}^{\hat{z}=50} = (-1, -7)$. The reason is that variation in contributions beyond this condition is not guaranteed, e.g., currently, Eq. (16) cannot account for the vector $\boldsymbol{\xi}_{\alpha}^{\hat{z}=20} = (4, 2)$. While a generalized solution can likely be achieved, such work exceeds the purposes of the present work. However, we note that with our approach presented in Fig. 3 (and relevant text), it is possible to correctly identify such contributions. Nevertheless, the general expression (17) allows interaction pressure tensors to be readily calculated numerically on a wide variety of lattice structures, including lattice structures such as Q49ZOTT in Fig. 1, as well as other shorter lattice structures such as the popular two-dimensional Q17 [8] and Q37 [46] [which are able to recover the equilibrium distribution function (6) up to third and fourth order, respectively]. In fact, Eq. (17) is also naturally applicable to high-isotropy-order forcing models developed initially for purposes of minimizing spurious currents [47], since Q49ZOTT shares most of the velocities with the 12th-order-isotropy force interaction model (see [43]). To demonstrate this we apply Eq. (17) (neglecting cross-interactions $\mathcal{G}^{\phi\varphi} = 0$) on the popular eighth-order-isotropy lattice structure (E8), which in fact covers all vectors in the second layer of Q49ZOTT ($z = 4, 5,$ and 8) as shown in Fig. 1. As shown in Appendix C, this leads to the same pressure tensor contributions derived by Shan [32]. In addition, we point out that most current methods of constructing high-order lattice structures operate on the basis of seeking the least populous group of vectors [48,49] and as such many high-order lattice structures do not contain any symmetry groups that comply with $\hat{z}$. Interested readers may refer to [8,11,37,48–50] for more details on high-order lattice models and [43,47] for details regarding high-isotropy-order forcing models.

Hereinafter we omit dimensional rank and refer to lattice models by their number of lattice velocities, e.g., Q49ZOTT. Force interaction lattices that are constructed for the sake of isotropy order, rather than the sake of recovering $\mathcal{O}$th-order terms in the equilibrium distribution function (6), will be referred to by their order of isotropy, e.g., for 12th-order isotropy (E12).

IV. CONTINUUM ANALYSIS

To assess and validate the definition of the interaction pressure tensor (17) on multiple high-order lattice structures, we need to obtain a general solution to the continuum approximation. In addition, as stated in the Introduction, such a solution also allows more convenient control of the model as it allows transport equations to be derived, an important feature that can allow high-order lattice models to be more readily applicable. These include solutions to the coexistence curve, equation of state, diffusion coefficients, interface profile, and surface tension. To approximate for the pressure tensor in the continuum limit two options are available, both of which require spatial derivatives to be approximated. Following previous work [43,51], we can approximate the spatial derivatives by Taylor expansion around $\psi(\boldsymbol{x} \pm \boldsymbol{\xi}_{\alpha} \Delta t)$,

$$
\begin{aligned}
\psi(\boldsymbol{x}+\boldsymbol{\xi}_{\alpha}\Delta t) \approx{} & \psi(\boldsymbol{x}) + \Delta t \xi_{\alpha,i}\partial_i\psi(\boldsymbol{x}) + \frac{\Delta t^2}{2!}\xi_{\alpha,i}\xi_{\alpha,j}\partial_i\partial_j\psi(\boldsymbol{x}) \\
& + \frac{\Delta t^3}{3!}\xi_{\alpha,i}\xi_{\alpha,j}\xi_{\alpha,k}\partial_i\partial_j\partial_k\psi(\boldsymbol{x}) + \cdots + \mathcal{O}^m.
\end{aligned}
$$
(18)

The first option, which is also the traditional approach [43,51], is to link the interaction force [e.g., Eq. (11)] to the interaction pressure tensor through the continuum derivatives using Eq. (2). Note that this also appears to be the most logical since, as stated earlier, the interaction force (11) is directly applicable on any lattice structure. This requires the approximation of the derivatives represented in $\sum_{\alpha} \tilde{w}_{\alpha} \psi(\boldsymbol{x}+\boldsymbol{\xi}_{\alpha}) \boldsymbol{\xi}_{\alpha}$ in the interaction force (11), obtained from applying the Taylor expansion (18). We will call this the standard solution for the continuum approximation of the interaction pressure tensor. This solution has already been shown in various previous works (readers may refer to [43] for full details) and here, for the sake of comparison, we provide the normal component (i.e., a one-dimensional problem with all gradients in x) of the standard solution, marked with an asterisk superscript,

$$
P_{xx}^{*(\mathrm{int})} = \mathcal{C}_2 \frac{\mathcal{G}}{2} \psi^2 + \mathcal{C}_4 \frac{\mathcal{G}}{4} \left[2\psi \frac{\partial^2 \psi}{\partial x^2} - \left(\frac{\partial \psi}{\partial x}\right)^2 \right]. \quad (19)
$$

The second approach is to approximate derivatives in the interaction pressure tensor at the discrete level directly, i.e., the derivatives representing the term $\sum_{\alpha} \tilde{w}_{\alpha} \psi(\boldsymbol{x}+\boldsymbol{\xi}_{\alpha}) \boldsymbol{\xi}_{\alpha} \boldsymbol{\xi}_{\alpha}$.

This requires prior knowledge of the discrete on-lattice pressure tensor from the definition (1). Having now provided (in Sec. III) a universal definition in Eq. (17) allows the second approach to be applied in a generalized way, which we demonstrate in this section.

Similar to the approach taken in Sec. III, we consider a key portion of the interaction pressure tensor individually based on the type of symmetry group. To this aim, as a starting point for our analysis, we consider any symmetry group $z \leqslant 2$, which, again, we classify by $\bar{z}$ and is defined at the discrete level by Eq. (13). The impact of $\bar{z}$ and $\hat{z}$ will be investigated in detail later in this section. Note that, similar to the preceding section, for typographical convenience, we use ψ to denote any form of pseudopotential throughout this section. We apply this expansion series (18) up to third-order derivatives directly in the on-lattice pressure tensor (13) and obtain (we omit the explicit dimensional dependence $\boldsymbol{x}$)

$$
\begin{aligned}
\mathcal{P}_{ij}^{\text{int}(\bar{z})} &= \frac{\mathcal{G}}{2} \psi \sum_{\alpha} \tilde{w}_{\alpha} \xi_{\alpha,i}^{\bar{z}} \xi_{\alpha,j}^{\bar{z}} \psi \left(\boldsymbol{x} + \boldsymbol{\xi}_{\alpha}^{\bar{z}} \right) \\
&\approx \frac{\mathcal{G}}{2} \psi \left(\sum_{\alpha} \tilde{w}_{\alpha} \xi_{\alpha,i}^{\bar{z}} \xi_{\alpha,j}^{\bar{z}} \psi + \Delta t \sum_{\alpha,k} \tilde{w}_{\alpha} \xi_{\alpha,i}^{\bar{z}} \xi_{\alpha,j}^{\bar{z}} \xi_{\alpha,k}^{\bar{z}} \partial_k \psi \right. \\
&\quad + \frac{\Delta t^2}{2!} \sum_{\alpha,k,l} \tilde{w}_{\alpha} \xi_{\alpha,i}^{\bar{z}} \xi_{\alpha,j}^{\bar{z}} \xi_{\alpha,k}^{\bar{z}} \xi_{\alpha,l}^{\bar{z}} \partial_{kl} \psi \\
&\quad + \frac{\Delta t^3}{3!} \sum_{\alpha,k,l,m} \tilde{w}_{\alpha} \xi_{\alpha,i}^{\bar{z}} \xi_{\alpha,j}^{\bar{z}} \xi_{\alpha,k}^{\bar{z}} \xi_{\alpha,l}^{\bar{z}} \xi_{\alpha,m}^{\bar{z}} \partial_{klm} \psi \\
&\quad \left. + \cdots + \mathcal{O}^m \right),
\end{aligned}
\tag{20}
$$

where the shorthand notation $\partial_{klm} = \partial_k \partial_l \partial_m$ is used. Notice that in this equation we absorbed directly the additional $\xi_{\alpha,i} \xi_{\alpha,j}$ terms, which come from the on-lattice pressure tensor.

If we identify that

$$
\sum_{\alpha} \tilde{w}_{\alpha} \xi_{\alpha,i} \xi_{\alpha,j} \cdots \xi_{\alpha,(\mathcal{O}^m)} = \mathcal{C}_m \triangle_{ij\cdots(\mathcal{O}^m)}^{(m)},
$$

then at any order of isotropy (m) we can remove the sum by the corresponding coefficient $\mathcal{C}_m$ and the isotropic delta function $\triangle_{ij\cdots(\mathcal{O}^m)}^{(m)}$ [43,52] (refer to Appendix B for details). Given that the isotropy conditions are already known, odd orders $m = 2n \pm 1$ sum to zero and related derivatives vanish. As such, we consider only even orders $m = 2n$ hereinafter. We are now left with zeroth-order and second-order derivatives [where first-order ∂_k and third-order ∂_{klm} derivatives in Eq. (20) vanish due to the aforementioned odd isotropy orders, namely, the third and fifth order of isotropy, respectively]. From Eq. (20) the continuum approximation of the total interaction pressure tensor (assuming that the entire lattice is made up of symmetry groups $z \leqslant 2$) is

$$
\mathcal{P}_{ij}^{\text{int}(z)} = \mathcal{C}_2 \frac{\mathcal{G}}{2} \psi^2 \delta_{ij} + \mathcal{C}_4 \frac{\mathcal{G}}{2} \frac{\Delta t^2}{2!} \psi \, \partial_{kl} \psi \, \triangle_{ijkl}^{(4)}.
\tag{21}
$$

Under the usual scenario of a one-dimensional problem (refer to Appendix A in [43]) with all gradients directed in x, such that $ijkl := x$, we obtain the normal component of Eq. (21),

$$
\mathcal{P}_{xx}^{\text{int}(z)} = \mathcal{C}_2 \frac{\mathcal{G}}{2} \psi^2 + 3 \mathcal{C}_4 \frac{\mathcal{G}}{4} \psi \frac{\partial^2 \psi}{\partial x^2}.
\tag{22}
$$

We recall that Eq. (20) accounts for only $\mathcal{P}_{ij}^{\text{int}(z)} \, \forall z \leqslant 2$ and is insufficient to define the pressure tensor on a lattice structure $z > 2$. It is however capable of completely describing the pressure tensor *on* the Q9 lattice structure. Using Q9 as an example here with corresponding coefficients $\mathcal{C}_2 = 1$ and $\mathcal{C}_4 = c_s^2 = \frac{1}{3}$ (see Appendix B) substituted into Eq. (22) then yields

$$
P_{xx}^{\text{int}} = \frac{\mathcal{G}}{2} \psi^2 + \frac{\mathcal{G}}{4} \psi \frac{\partial^2 \psi}{\partial x^2},
\tag{23}
$$

which was already found in [32]. The result was also found in [34] [see Eq. (13) therein], where the only difference is the constant $\frac{1}{6}$ appearing in front of the term $\mathcal{G} \psi \frac{\partial^2 \psi}{\partial x^2}$. The different constant is due to the fourth-order-isotropy coefficient in [34] set to $\mathcal{C}_4/2 = c_s^4$.

Comparing Eq. (23) against the standard continuum approximation $P_{xx}^{*(\text{int})}$ [Eq. (19)] obtained from the interaction force (11) directly, we see that $P_{xx}^{*(int)}$ includes an extra first-order derivative term $\frac{\partial \psi}{\partial x}$. As mentioned in the Introduction, the Q9 lattice has insufficient interaction vectors to be consistent with the theory in Eq. (2) [32,34]; however, perplexingly, the on-lattice pressure tensor (13) is exact for $z < 2$ [34]. According to Shan [32], increasing the interaction range results in the on-lattice pressure tensor to include this mix of first-order $(\partial_i \psi)^2$ and second-order $\psi \partial_{ij} \psi$ derivatives.

The following question then arises: Does the proposed general expression (17) produce the correct continuum approximation? We answer the question in the affirmative, which we demonstrate here. To this aim, we consider the additional contributions that appear for symmetry groups $z > 2$, but only the portions, say, $\mathcal{Z} \in (\bar{z}, \hat{z})$, of the pressure tensor where we have interaction terms that involve sums of the general form

$$
\mathcal{P}_{ij}^{\text{int}(\mathcal{Z})}(\boldsymbol{x}) = \mathcal{G} \sum_{\alpha} \frac{\tilde{w}_{\alpha}}{2 \mathcal{E}^{\mathcal{Z}}} \left[\psi \left(\boldsymbol{x} - \boldsymbol{e}_{\alpha}^{\text{A}} \right) \psi \left(\boldsymbol{x} + \boldsymbol{e}_{\alpha}^{\text{B}} \right) \right] \xi_{\alpha,i}^{\mathcal{Z}} \xi_{\alpha,j}^{\mathcal{Z}}, \tag{24}
$$

where the sum of $\boldsymbol{e}_{\alpha}^{\text{A}}$ and $\boldsymbol{e}_{\alpha}^{\text{B}}$, of any form (axial, diagonal, or mixed), will be equal to the length of $\boldsymbol{\xi}_{\alpha}^{\mathcal{Z}}$, i.e., $|\boldsymbol{\xi}_{\alpha}^{\mathcal{Z}}| = |\boldsymbol{e}_{\alpha}^{\text{A}}| + |\boldsymbol{e}_{\alpha}^{\text{B}}|$. The above is essentially a simplified general expression for the two last terms in both Eqs. (15) and (16) with $\beta = 1$. Applying the Taylor expansion to the term in square brackets in Eq. (24) up to second-order derivatives,

$$
\begin{aligned}
\mathcal{P}_{ij}^{\text{int}(\mathcal{Z})}(\boldsymbol{x}) \approx \mathcal{G} \sum_{\alpha} \frac{\tilde{w}_{\alpha}}{2 \mathcal{E}^{\mathcal{Z}}} \xi_{\alpha,i}^{\mathcal{Z}} \xi_{\alpha,j}^{\mathcal{Z}} &\left(\left[\psi(\boldsymbol{x}) - \Delta t \, \partial_k \psi(\boldsymbol{x}) e_{\alpha,k}^{\text{A}} + \frac{\Delta t^2}{2!} \partial_{kl} \psi(\boldsymbol{x}) e_{\alpha,k}^{\text{A}} e_{\alpha,l}^{\text{A}} \right] \right. \\
&\left. \times \left[\psi(\boldsymbol{x}) + \Delta t \, \partial_k \psi(\boldsymbol{x}) e_{\alpha,k}^{\text{B}} + \frac{\Delta t^2}{2!} \partial_{kl} \psi(\boldsymbol{x}) e_{\alpha,k}^{\text{B}} e_{\alpha,l}^{\text{B}} \right] \right),
\end{aligned}
$$

and multiplying through both sets of expansion, we obtain (negative signs are already absorbed)

$$
\mathcal{G} \sum_{\alpha} \frac{\tilde{w}_{\alpha}}{2\mathcal{E}^{\mathcal{Z}}} \xi^{\mathcal{Z}}_{\alpha,i} \xi^{\mathcal{Z}}_{\alpha,j} \Bigg[(\psi)^2 + \Delta t \, \psi \big[\partial_k \psi \, e^{\mathrm{B}}_{\alpha,k} - \partial_k \psi \, e^{\mathrm{A}}_{\alpha,k} \big] + \frac{\Delta t^2}{2!} \psi \big[\partial_{kl} \psi \, e^{\mathrm{B}}_{\alpha,k} e^{\mathrm{B}}_{\alpha,l} + \partial_{kl} \psi \, e^{\mathrm{A}}_{\alpha,k} e^{\mathrm{A}}_{\alpha,l} \big]
$$

$$
- \Delta t^2 (\partial_k \psi)^2 e^{\mathrm{A}}_{\alpha,k} e^{\mathrm{B}}_{\alpha,k} + \Delta t \frac{\Delta t^2}{2!} \big[\partial_k \psi \, \partial_{kl} \psi \, e^{\mathrm{B}}_{\alpha,k} e^{\mathrm{A}}_{\alpha,k} e^{\mathrm{A}}_{\alpha,l} - \partial_k \psi \, \partial_{kl} \psi \, e^{\mathrm{A}}_{\alpha,k} e^{\mathrm{B}}_{\alpha,k} e^{\mathrm{B}}_{\alpha,l} \big]
$$

$$
+ \left(\frac{\Delta t^2}{2!} \right)^2 (\partial_{kl} \psi)^2 e^{\mathrm{A}}_{\alpha,k} e^{\mathrm{A}}_{\alpha,l} e^{\mathrm{B}}_{\alpha,k} e^{\mathrm{B}}_{\alpha,l} \Bigg].
$$

After rearranging and removing odd isotropy orders (that sum to zero) related to, namely, the product of mixed derivatives $\psi \partial_k \psi$ and $\partial_k \psi \, \partial_{kl} \psi$, we obtain

$$
\mathcal{P}^{\mathrm{int}(\mathcal{Z})}_{ij} = \mathcal{G} \sum_{\alpha} \frac{\tilde{w}_{\alpha}}{2\mathcal{E}^{\mathcal{Z}}} \big[\psi(\boldsymbol{x} - \boldsymbol{e}^{\mathrm{A}}_{\alpha}) \cdot \psi(\boldsymbol{x} + \boldsymbol{e}^{\mathrm{B}}_{\alpha}) \big] \xi^{\mathcal{Z}}_{\alpha,i} \xi^{\mathcal{Z}}_{\alpha,j}
$$

$$
\approx \mathcal{G} \frac{1}{2\mathcal{E}^{\mathcal{Z}}} \Bigg[\sum_{\alpha} \tilde{w}_{\alpha} (\psi)^2 \xi^{\mathcal{Z}}_{\alpha,i} \xi^{\mathcal{Z}}_{\alpha,j} - \Delta t^2 \sum_{\alpha,k} \tilde{w}_{\alpha} (\partial_k \psi)^2 e^{\mathrm{A}}_{\alpha,k} e^{\mathrm{B}}_{\alpha,k} \xi^{\mathcal{Z}}_{\alpha,i} \xi^{\mathcal{Z}}_{\alpha,j}
$$

$$
+ \frac{\Delta t^2}{2!} \sum_{\alpha,k,l} \tilde{w}_{\alpha} \psi \big[\partial_{kl} \psi \, e^{\mathrm{B}}_{\alpha,k} e^{\mathrm{B}}_{\alpha,l} + \partial_{kl} \psi \, e^{\mathrm{A}}_{\alpha,k} e^{\mathrm{A}}_{\alpha,l} \big] \xi^{\mathcal{Z}}_{\alpha,i} \xi^{\mathcal{Z}}_{\alpha,j} + \left(\frac{\Delta t^2}{2!} \right)^2 \sum_{\alpha,k,l} \tilde{w}_{\alpha} (\partial_{kl} \psi)^2 e^{\mathrm{A}}_{\alpha,k} e^{\mathrm{A}}_{\alpha,l} e^{\mathrm{B}}_{\alpha,k} e^{\mathrm{B}}_{\alpha,l} \xi^{\mathcal{Z}}_{\alpha,i} \xi^{\mathcal{Z}}_{\alpha,j} \Bigg]. \tag{25}
$$

We now have terms related to the second, fourth, and sixth order of isotropy and consequently obtain zeroth-, first-, and second-order derivatives.[3] Most important is that the first derivative ∂_k, which previously vanished due to odd isotropy order in Eq. (20), is now present as a result of the increase in isotropy gradient. Notice that this is negative due to the expansion $\boldsymbol{x} - \boldsymbol{e}_{\alpha}$. As such, the continuum approximation of Eq. (24) in general form is

$$
\mathcal{P}^{\mathrm{int}(\mathcal{Z})}_{ij} = \frac{\mathcal{G}}{2\mathcal{E}^{\mathcal{Z}}} \left(\mathcal{C}_2 \psi^2 \delta_{ij} - \mathcal{C}_4 \Delta t^2 (\partial_k \psi)^2 \triangle^{(2)}_{kk} \triangle^{(2)}_{ij} + \mathcal{C}_4 \frac{2\Delta t^2}{2!} \psi \, \partial_{kl} \psi \, \triangle^{(2)}_{kl} \triangle^{(2)}_{ij} + \mathcal{C}_6 \frac{\Delta t^4}{4} (\partial_{kl} \psi)^2 \triangle^{(4)}_{kkll} \triangle^{(2)}_{ij} \right), \tag{26}
$$

where $\mathcal{C}_m$ are unique coefficients for $\mathcal{P}^{(\mathcal{Z})}_{ij}$ that describe the fragment of coefficients from the contribution from a portion $\mathcal{Z}$ of sum lattice weights at any given order of isotropy (m), i.e., $\sum_{\alpha} \tilde{w}_{\alpha} e_{\alpha,(\mathcal{O}^{m-2})} \xi^{\mathcal{Z}}_{\alpha,i} \xi^{\mathcal{Z}}_{\alpha,j} = \mathcal{C}_m \triangle^{(m-2)}_{\cdots \mathcal{O}^{m-2}} \triangle^{(2)}_{ij}$.

For the sake of completeness, the normal component of Eq. (26) is

$$
\mathcal{P}^{\mathrm{int}(\mathcal{Z})}_{xx} = \frac{\mathcal{G} \mathcal{C}_2}{2\mathcal{E}^{\mathcal{Z}}} \psi^2 + \frac{\mathcal{G} \mathcal{C}_4}{2\mathcal{E}^{\mathcal{Z}}} \left[\psi \frac{\partial^2 \psi}{\partial x^2} - \left(\frac{\partial \psi}{\partial x} \right)^2 \right], \tag{27}
$$

where in order to directly compare against Eq. (19) we have left out the sixth-order isotropy related to the term $(\partial_{ij} \psi)^2$. Evidently, we have demonstrated that indeed the additional contributions, i.e., $\psi(\boldsymbol{x} - \boldsymbol{e}^{\mathrm{A}}_{\alpha}) \cdot \psi(\boldsymbol{x} + \boldsymbol{e}^{\mathrm{B}}_{\alpha})$, that are present at interaction range $z > 2$ introduce an additional derivative in the interaction pressure tensor.

Upon summing all contributions from all various symmetry groups z [i.e., Eq. (12)], including the additional contributions $\mathcal{P}^{(\mathcal{Z})}_{ij}$ [such as Eq. (26) above], then $\mathcal{C}_2/2\mathcal{E}^{\mathcal{Z}}$ will reduce to $\sum_{\mathcal{Z}} \mathcal{C}^{(\mathcal{Z})}_2/2\mathcal{E}^{\mathcal{Z}} = \mathcal{C}_2/2$. However, the same does not hold for $\mathcal{C}_4$. Instead, we can present a generalized form of the continuum approximation of the total interaction pressure tensor truncated up to fourth-order isotropy gradients (normal component for the sake of consistency)

$$
P^{\mathrm{int}}_{xx} = \sum_z \mathcal{P}^{\mathrm{int}(z)}_{xx} = \mathcal{G} \frac{\mathcal{C}_2}{2} \psi^2 + \mathcal{G} \left[\mathcal{A} \psi \frac{\partial^2 \psi}{\partial x^2} - \mathcal{B} \left(\frac{\partial \psi}{\partial x} \right)^2 \right]. \tag{28}
$$

For the sake of completeness, we provide the solution of the above in terms of a nonideal fluid mixture; including intra- and inter-interactions as done in Eq. (17) and using the same notation, Eq. (28) then takes the form

$$
P^{\mathrm{int}}_{xx} = \sum_{\phi}^{\mathcal{S}} \sum_z \mathcal{P}^{\phi,\mathrm{int}(z)}_{xx} = \sum_{\phi}^{\mathcal{S}} \Bigg\{ \mathcal{G}^{\phi\phi} \frac{\mathcal{C}_2}{2} (\psi^{\phi})^2 + \mathcal{G}^{\phi\phi} \left[\mathcal{A} \psi^{\phi} \frac{\partial^2 \psi^{\phi}}{\partial x^2} - \mathcal{B} \left(\frac{\partial \psi^{\phi}}{\partial x} \right)^2 \right]
$$

$$
+ \sum_{\varphi \neq \phi}^{\mathcal{S}} \left(\mathcal{G}^{\phi\varphi} \frac{\mathcal{C}_2}{2} \Psi^{\phi} \Psi^{\varphi} + \mathcal{G}^{\phi\varphi} \left[\mathcal{A} \Psi^{\phi} \frac{\partial^2 \Psi^{\varphi}}{\partial x^2} - \mathcal{B} \frac{\partial \Psi^{\phi}}{\partial x} \frac{\partial \Psi^{\varphi}}{\partial x} \right] \right) \Bigg\}. \tag{29}
$$

---

[3]The even order of isotropy from terms in Eq. (25) is explicitly (for brevity we omit here the dependence on $\mathcal{Z}$), for second order, $\xi_{\alpha,i} \xi_{\alpha,j}$; for fourth order, $-e^{\mathrm{A}}_{\alpha,k} e^{\mathrm{B}}_{\alpha,k} \xi_{\alpha,i} \xi_{\alpha,j} = \frac{-\xi_{\alpha,k}}{2} \frac{\xi_{\alpha,k}}{2} \xi_{\alpha,i} \xi_{\alpha,j}$, returning a negative constant, and $(e^{\mathrm{A}}_{\alpha,k} e^{\mathrm{A}}_{\alpha,l} + e^{\mathrm{B}}_{\alpha,k} e^{\mathrm{B}}_{\alpha,l}) \xi_{\alpha,i} \xi_{\alpha,j} = (\frac{-\xi_{\alpha,k} - \xi_{\alpha,l}}{4} + \frac{\xi_{\alpha,k} \xi_{\alpha,l}}{4}) \xi_{\alpha,i} \xi_{\alpha,j}$, returning a positive constant; and finally for sixth order, $e^{\mathrm{A}}_{\alpha,k} e^{\mathrm{A}}_{\alpha,l} e^{\mathrm{B}}_{\alpha,k} e^{\mathrm{B}}_{\alpha,l} \xi_{\alpha,i} \xi_{\alpha,j} = (\frac{-\xi_{\alpha,k}}{2} \frac{-\xi_{\alpha,l}}{2})(\frac{\xi_{\alpha,k}}{2} \frac{\xi_{\alpha,l}}{2}) \xi_{\alpha,i} \xi_{\alpha,j}$, returning also a positive constant.

The coefficients $\mathcal{A}$ and $\mathcal{B}$ account for all additional variations of $\mathbb{C}_4$ for the various arbitrary portions of the pressure tensor $\mathcal{P}_{ij}^{\text{int}(z)}$; $\mathcal{B}$ appears only for $z > 2$ [e.g., Eq. (26)]. Since both $\mathcal{A}$ and $\mathcal{B}$ are related to fourth-order isotropy, both are proportional to $\mathcal{C}_4$ and, given the analysis above, $\mathcal{A} \neq \mathcal{B}$. Fortunately, by summing all contributions [e.g., Eqs. (21) and (26)] for various lattices according to the procedure above, it was found that

$$\mathcal{A} = \frac{6\mathcal{C}_4 + \mathcal{C}_2}{12}, \tag{30a}$$

$$\mathcal{B} = \frac{3\mathcal{C}_4 - \mathcal{C}_2}{12} \tag{30b}$$

hold on all lattice structures tested in this work (all lattices presented in Sec. V) and it is expected that (30) holds for any other lattice structure. The solution (30) coincides exactly with the coefficients appearing in the continuum approximation derived for the E8 lattice in [32] [see Eq. (22) therein], with the condition that $\mathcal{C}_2 = 1$. Furthermore, it was also found that both Q49ZOTT and the 12th-order isotropy forcing model in [43] do not converge to the solution (30) *unless* contributions $\boldsymbol{F}_2$ and $\boldsymbol{F}_3$ (as illustrated in Fig. 3) are factored in accordance with requirements (16) detailed in Sec. III A. Here the $\mathcal{C}_2$ in Eq. (30) allow $\mathcal{A}$ and $\mathcal{B}$ to be determined in the case of $\mathcal{C}_2 \neq 1$, e.g., in many traditional applications of SC pseudopotentials $\mathcal{C}_2 = \sum_\alpha \tilde{w}_\alpha \xi_{\alpha,i} \xi_{\alpha,i} = c_s^2$ since these were applied directly on the Q9 lattice. In addition, we point out that with interactions directly on the Q9 lattice (exclusively), the solution (30) will result in $\mathcal{B}$ always being equal to zero, regardless of isotropy conditions, and Eq. (28) will then reduce exactly to Eq. (23). The standard solution $P_{xx}^{*\text{int}}$ [Eq. (19)] suggests $\mathcal{A} = 2\mathcal{B} = \mathcal{C}_4/2$; however, from the analysis above, this is evidently incorrect. We further compare their accuracy numerically in Sec. V. To close, the continuum approximation to the exact discrete definition (17), up to fourth-order isotropy gradients, is shown to surprisingly have a generalized form defined in Eqs. (28) and (30).

A. Thermodynamic consistency

With the definitions in Eqs. (9) and (28), it is now possible to directly assess the thermodynamic consistency following [27,32,36]. For a single-component liquid-gas system in a one-dimensional interface with gradients only in x, the normal component of the pressure tensor is constant $P_{xx}^{\text{tot}} = P_c$ across both phases. Using the relation $\partial_{xx}\psi = \frac{1}{2}\partial_\psi(\partial_x\psi)^2$, it is possible to integrate Eq. (28),

$$\frac{\mathcal{G}(d\psi/d\rho)^2}{8(1-\epsilon)\psi^\epsilon}\left(\frac{\partial\rho}{\partial x}\right)^2 = \int\left(P_c - \rho c_s^2 - \mathcal{G}\frac{\mathcal{C}_2}{2}\psi^2\right)\frac{d\psi}{d\rho}\frac{1}{\psi^{1+\epsilon}}\,d\rho, \tag{31}$$

where the coefficient ϵ with Eq. (30) is defined by

$$\epsilon = \frac{2\mathcal{B}}{\mathcal{A}} = \frac{6\mathcal{C}_4 - 2\mathcal{C}_2}{6\mathcal{C}_4 + \mathcal{C}_2}. \tag{32}$$

Since there are no density gradients in the bulk of each phase (i.e., $\frac{\partial\rho}{\partial x} = 0$ for gas $\rho = \rho_g$ and liquid $\rho = \rho_l$), to satisfy mechanical equilibrium on the lattice the integral over the two

phases ρ_g and ρ_l has the constraint

$$\int_{\rho_g}^{\rho_l}[P_c - P_0(\rho,\mathcal{G})]\frac{d\psi}{d\rho}\frac{1}{\psi^{1+\epsilon}}\,d\rho = 0, \tag{33}$$

where the equation of state $P_0(\rho,\mathcal{G}) = \rho c_s^2 + \mathcal{G}\frac{\mathcal{C}_2}{2}\psi^2$. Satisfying Eq. (33) requires the equation of state in both phases to be equal $P_0(\rho_g,\mathcal{G}) = P_0(\rho_l,\mathcal{G}) = P_c$. Moreover, the Maxwell construction (thermodynamic consistency) can be defined by (see. e.g., [51])

$$\int_{\rho_g}^{\rho_l}[P_c - P_0(\rho,\mathcal{G})]\frac{1}{\rho^2}\,d\rho = 0, \tag{34}$$

which allows for the coexistence density of each phase (ρ_g and ρ_l) to be approximated theoretically.

The lattice mechanical equilibrium condition (33) will conform with the Maxwell construction (34) depending on the choice of ψ. For example, if we choose to set $\psi = \rho^0(1 - e^{-\rho/\rho^0})$, then $d\psi/d\rho = e^{-\rho/\rho^0}$, or if $\psi = e^{-1/\rho}$, then $d\psi/d\rho = e^{-1/\rho}/\rho^2$. According to Eq. (33), the former is thermodynamically inconsistent [51,53]. The latter, for the Q9 lattice where $\mathcal{B} = 0$ (and thus $\epsilon = 0$), does in fact satisfy thermodynamic consistency (34), which we can demonstrate in Eq. (33) by $\frac{d\psi}{d\rho}\psi^{-1-\epsilon} = 1/\rho^2$ [32,36,53]. This, however, is not the case for higher-order isotropy lattices since $\epsilon > 0$. Sbragaglia and Shan [36] addressed this issue and proposed a general pseudopotential that satisfies thermodynamic consistency,

$$\psi = \left(\frac{\rho}{\epsilon + \rho}\right)^{1/\epsilon}. \tag{35}$$

In Fig. 4 we calculate the theoretical thermodynamic phase coexistence (34) of Q9 with $\psi = e^{-1/\rho}$ and Q49ZOTT using Eqs. (30) and (35) (refer to [27] for details on the procedure). The theoretical predictions are then compared against their equilibrium bulk phase coexistence densities obtained numerically for a range of interaction strengths beyond the critical limit $\mathcal{G}/G_{\text{crit}} > 1$ (refer to details in Fig. 4). The critical interaction strength G_{crit} is the limit at which phase separation occurs in a single-component two-phase system, which is defined by $dP_0/d\rho = 0$. As can be seen in Fig. 4, both the Q9 and Q49ZOTT lattices are shown to satisfy thermodynamic consistency (34). In addition, although not shown here, we also found using $\psi(\rho) = e^{-1/\rho}$ with Q49ZOTT to be thermodynamically inconsistent. In Fig. 4(b) we see a slight deviation for Q49ZOTT for $\mathcal{G}/G_{\text{crit}} > 1.125$, where the absolute relative error remains less than 0.6% for ρ_l and less than 2.5% for ρ_g, with the largest deviation at G_{max}. However, these are similar to the deviations reported in [36] using Q9 with E8. As suggested in [36], these deviations could be the result of a thin interface, which becomes thinner with increasing $\mathcal{G}/G_{\text{crit}}$, which may require higher-order approximations in the Taylor expansion.

As a final note on thermodynamic consistency we mention that the standard solution (19), as stated earlier, suggests that $\mathcal{A} = 2\mathcal{B} = \mathcal{C}_4/2$, for which Eq. (32) results in $\epsilon = 1$. According to the standard solution, this suggests that mechanical equilibrium (33) can only satisfy Eq. (34) if $\psi \approx \rho$ [51]. In agreement with [32,36], from our analysis above and the results for Q9 with $\psi = e^{-1/\rho}$ in Fig. 4(a), the definition
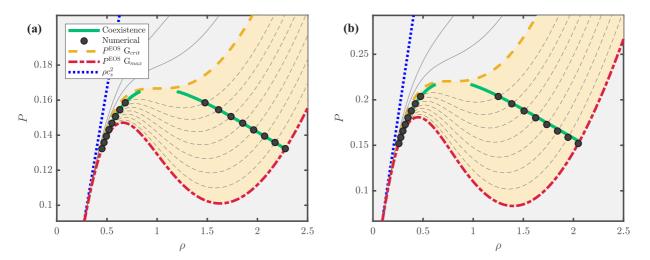
FIG. 4. Theoretical prediction of equation of state P_0 (dashed and dotted curved lines) for a range of $\mathcal{G}/G_{\text{crit}}$ up to $G_{\text{max}} = 1.225G_{\text{crit}}$ (red dot-dashed line), solved for (a) the Q9 lattice model ($\epsilon = 0$) with $\psi(\rho) = e^{-1/\rho}$ and (b) the Q49ZOTT lattice model with Eqs. (30) and (35). The thermodynamic coexistence curve (bold solid green line) drawn within the shaded region is obtained from the Maxwell construction (34). Numerical simulations were conducted for $\mathcal{G}/G_{\text{crit}} = \{1.05, 1.075, 1.1, 1.125, 1.15, 1.175, 1.2, G_{\text{max}}\}$ where the bulk properties of each phase (●), namely, densities and corresponding static pressure, are obtained from Eqs. (7a), (9), and (17).

$\psi \approx \rho$ is not a valid pseudopotential to describe a single-component liquid-gas system.

B. Surface tension

The surface tension coefficient is an important transport property in many applications with nonideal fluids and is a fitting candidate for checking the validity of the interaction pressure tensor (17). The surface tension between components over a one-dimensional interface with all gradients in x can be described by the Bakker formula [31,54]

$$\sigma = \int_{-\infty}^{+\infty} \left(P_N^{\text{tot}} - P_T^{\text{tot}} \right) dx, \quad (36)$$

where the normal component $P_N^{\text{tot}} = P_{xx}^{\text{tot}} = P_{xx}^{\text{kin}} + P_{xx}^{\text{int}}$ and tangential component $P_T^{\text{tot}} = P_{yy}^{\text{tot}} = P_{yy}^{\text{kin}} + P_{yy}^{\text{int}}$ [27,43,51,55]. The total momentum flux tensor P_{ij}^{tot} is obtained from Eq. (9). With Eq. (17) we can numerically solve for the surface tension (36) directly. Likewise, with the continuum approximation (29) and (30) defined, a theoretical approximation of the surface tension can be derived for a multicomponent system with all interactions included. To this end, taking the mismatch between normal and tangential components of the total pressure tensor (9), (29), and (30) and assuming a one-dimensional interface with all gradients along x, we obtain (see [32,43])

$$\sigma = -\sum_{\phi}^{\mathcal{S}} \left(\mathcal{Y}_4 \mathcal{G}^{\phi\phi} \int \left(\frac{\partial \psi^\phi}{\partial x} \right)^2 dx \right.$$

$$\left. + \sum_{\varphi \neq \phi}^{\mathcal{S}} \mathcal{Y}_4 \mathcal{G}^{\phi\varphi} \int \left(\frac{\partial \Psi^\phi}{\partial x} \right) \left(\frac{\partial \Psi^\varphi}{\partial x} \right) dx \right). \quad (37)$$

The constant $\mathcal{Y}_4$ is a combination of fragments of the various coefficients [i.e., $\mathcal{A}$ and $\mathcal{B}$ from Eq. (30)] left over from taking the mismatch between the normal and tangential components. However, using the same concept as Eq. (24)

and collecting all various z contributions [e.g., Eq. (25)], a consistent solution is found,

$$\mathcal{Y}_{(m)} \triangle_{\cdots\mathcal{O}^{m-2}}^{(m-2)} = \sum_\alpha \tilde{w}_\alpha (e_{\alpha,i})^{m-2} (\xi_{\alpha,i} \xi_{\alpha,i} - \xi_{\alpha,j} \xi_{\alpha,j}), \quad (38)$$

where derivatives are directed in i and $e_{\alpha,i} = \xi_{\alpha,i}/2$. In Eq. (37) terms are related to fourth-order isotropy, thus $m = 4$, solving Eq. (38),

$$\mathcal{Y}_4 \triangle_{xx}^{(2)} = \mathcal{Y}_4 = \sum_\alpha \tilde{w}_\alpha (e_{\alpha,x})^2 (\xi_{\alpha,x} \xi_{\alpha,x} - \xi_{\alpha,y} \xi_{\alpha,y}) = \frac{\mathcal{C}_4}{2},$$

where $\triangle_{xx}^{(2)} = \delta_{xx} = 1$ since in Eq. (37) derivatives are directed in x. This subsequently allows Eq. (37) to coincide with previous continuum approximations of the surface tension [27,32,33,43,51]. It is also interesting to note that for the flat interface, with Eqs. (29) and (30), the derived surface tension coefficient in (37) and (38) has essentially the same form as the one obtain with the standard solution (19) (see, e.g., [43]). Furthermore, we show that Eq. (38) holds for high-order terms. To demonstrate this we consider sixth-order isotropy $m = 6$, which was neglected previously in Eq. (27), and then the constant $\mathcal{Y}_6$, which is related to the additional derivative $(\partial_{ij} \psi)^2$ in Eq. (26), can be defined directly using Eq. (38),

$$\mathcal{Y}_6 \triangle_{xxxx}^{(4)} = 3\mathcal{Y}_6 = \sum_\alpha \tilde{w}_\alpha (e_{\alpha,x})^4 (\xi_{\alpha,x} \xi_{\alpha,x} - \xi_{\alpha,y} \xi_{\alpha,y}),$$

which yields

$$\mathcal{Y}_6 = \frac{\mathcal{C}_6}{4}.$$

This also coincides exactly with that found in a separate study by Sbragaglia *et al.* [33] on the conventional eighth-order-isotropy force interaction stencil. Note that Eq. (38) only holds up to the same mth order of isotropy as that of the given lattice structure.

C. Closing remarks

We point out that the definition for the interaction force (11) is not dependent on the lattice structure; however, the same is not true for the consequent interaction pressure tensor based on the discrete definition (1). For example, consider two lattice structures with identical accuracy and sound speed c_s, such as Q25ZOT [37] and Q17ZOT [48], which have not only different velocities but also different sets of symmetry groups where, unlike Q25ZOT, the Q17ZOT lattice structure does not have any vectors with mixed components ($\hat{z}$) and as such does not require Eq. (16). Hence, at the discrete level their form is different. Fortunately, as we have shown here, the continuum approximation of this discrete definition can be generalized by Eqs. (29) and (30), allowing the interaction pressure tensor for Q25ZOT and Q17ZOT to be defined in the same form at the continuum limit. This is important, because this allows us to identify key equilibrium transport properties as we have shown in previous sections, namely, thermodynamic consistency in a single-component liquid-gas system, the equation of state, and the surface tension coefficient, as well as other properties which are beyond the scope of the present work.

V. NUMERICAL EXPERIMENT AND DISCUSSION

To test the validity of the general expression for the interaction pressure tensor (17) and its continuum approximation (29) and (30) for a variety of high-order lattice structures, we consider two common test cases, namely, the flat-interface test and a circular interface, by considering a single-droplet immersed in a fluid. Note that all results presented throughout this section are in lattice units.

The initial density field for both cases is achieved using a hyperbolic tangent function [20]. This allows for a smooth initial interface, preventing potential instabilities at the start of the simulations associated with sharp gradients. We defer details of the functions used for the initial density field to Appendix D. The computational domain $x = (n_x, n_y)$ for the flat interface was set to $x = (200, 8)$ with initial interface width $W_0 = 10$ and for the circular droplet test $x = (100, 100)$ with $W_0 = 5$. Other than geometric and stability purposes, the initial conditions for tests conducted here are unimportant since the simulations will converge towards equilibrium based on the interactions, i.e., although an initial interface width W_0 can be set, the actual final width is purely dependent on model parameters. We emphasize that the numerical accuracy, stability, and efficiency between the various lattice structures are *not* compared in detail as this is beyond the scope of the present work. For the reasons above, the size of the computational domain and initial interface width is kept the same for all lattice structures tested. For all tests the total pressure tensor P_{xx}^{tot} is obtained from the definition (9), with the kinetic part obtained from Eq. (10) at equilibrium and the interaction part obtained using different solutions, namely, numerical results from Eq. (17) and its continuum approximation defined in Eqs. (29) and (30), and the standard solution given in Eq. (19). Here the total pressure tensor with these solutions to the interaction part will be denoted by P_{xx}, P_{xx}^{CA}, and $P_{xx}^{*\text{CA}}$, respectively, where the notation CA refers to the continuum

approximation and the asterisk is used to identify the standard solution.

A. Flat interface

A unique feature of the one-dimensional flat-interface test is that, although the pressure tensor is anisotropic at the interface, the normal component P_{xx} will remain constant [31] due to the absence of tensorial ambiguity in the problem [43]. In our first test, we check this fundamental aspect of the normal component of the pressure tensor P_{xx} and compare the general expression (17) and its continuum approximation (29) and (30) directly against the standard P_{ij}^* solution (19), commonly used in the literature (see, e.g., [26,35]). To do this, we first use Q9 directly on the lattice and in addition to this with the higher-isotropy-order lattice structures, namely, 24, 36, and 48 lattice interaction vectors, which comply with eighth-order (E8), tenth-order (E10), and 12th-order (E12) isotropy (for details refer to [43]). Motivation for this follows previous works where Sbragaglia and Belardinelli [34] demonstrated the constant P_{xx} profile along a flat interface with the Q9 lattice (exclusively) and E8 since it was used in the introduction of the exact lattice theory by Shan [32]. Hence, we extend previous works by deploying Q9 with E10 and E12, which in turn allows us to demonstrate the universality of Eqs. (17), (29), and (30). In this test, the initial densities in the bulk of each phase are $\rho_0^\phi = \rho_0^\varphi = 1$ and viscosities are set to $\tau^\phi = \tau^\varphi = 1.2$. Only inter-interactions $\mathcal{G}^{\phi\varphi}$ are considered with the pseudopotential form $\Psi^\phi = \rho^0(1 - e^{-\rho^\phi/\rho^0})$, where we set $\rho^0 = 0.4$ to refine the interface resolution [43]. We set the inter-interaction strength to some value above the immiscible limit, which is the point where the mutual diffusion between two fluid components is negative [40]. Following [40], we approximate this by $\mathcal{G}^{\phi\varphi} \approx c_s^2 4/\mathcal{C}_2[\Psi^\phi + \Psi^\varphi]$, where the additional $c_s^2/\mathcal{C}_2$ is included to match strengths between various lattices (since $\mathcal{C}_2$ is not set to unity in [40]). The results are presented in Fig. 5. From Fig. 5(a) it is clear that the numerical calculation (17) and its continuum approximation (29) and (30) are constant throughout the interface, whereas the standard solution (19) is not. We recall that Eqs. (29) and (30) directly on the Q9 lattice will reduce to Eq. (23) since $\mathcal{B} = 0$. The results for Q9 with E8, in Fig. 5(b), again demonstrate the accuracy of the numerical calculation (17), with a constant P_{xx} profile throughout the interface, although it is clear that its continuum approximation (29) and (30), truncated at fourth-order isotropy gradients, which starts to deviate, is still more accurate than the standard solution (19). In Fig. 5(c) the constant profile of P_{xx} is tested explicitly by calculating the spatial variation $\Delta P_{xx}\%$ of the numerical (17). Here $\Delta P_{xx}\%$ is defined by comparing P_{xx} along x against some constant reference value $P_{xx}(x)$, where we have chosen this to be at center $x = 100$ in the bulk of fluid ϕ. At the level of deviation seen in Fig. 5(c) (we recall that it is on order of $1 \times 10^{-13}\%$) the P_{xx} profiles for Q9 on the lattice, and with E8, E10, and E12 interaction models, can all be deemed to be constant throughout the interface up to machine accuracy.

We then move on to conduct the same test on higher-order lattices, which can be seen for the ZOT construction Q25ZOT (for details refer to [37]) in Fig. 6(a). Visually, the numerical
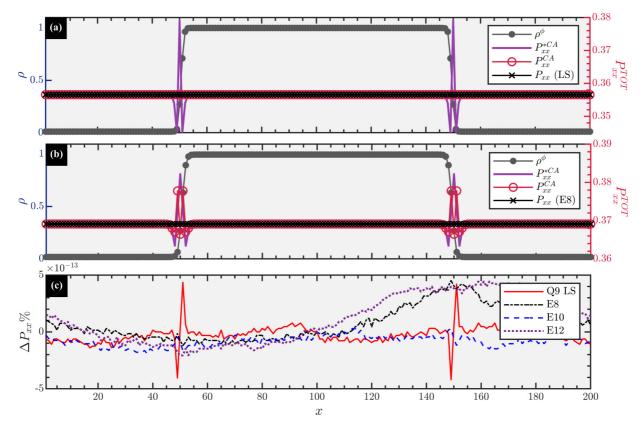
FIG. 5. Numerical results at equilibrium for the flat-interface test using the Q9 lattice model. The pseudopotential interactions (11) are deployed (a) directly on the lattice structure (LS) and (b) with the E8 model. The interaction component of P_{xx}^{tot} obtained numerically P_{xx} ($\times$) from Eq. (17) and its continuum approximation P_{xx}^{CA} ($\circ$) obtained from Eqs. (29) and (30) are compared against the standard solution $P_{xx}^{*\text{CA}}$ (solid line) from Eq. (19). (c) Constancy $\Delta P_{xx}\%$ of the P_{xx} obtained numerically (17), tested for the Q9 LS, E8, E10, and E12 along spatial dimension x. For each lattice, the constancy $\Delta P_{xx}\%$ is calculated as the percentage difference of P_{xx} along x against the reference $P_{xx}(x)$ measured at center $x = 100$.

calculation (17) appears to be a constant interface, whereas some deviation is seen for its continuum approximation (29) and (30). This observation is similar to that made for Q9 with E8 although not as severe, which is likely due to the lower isotropy order of Q25ZOT (sixth order) compared to E8 (eight order). This suggests that higher-order lattices require higher-order approximations in the continuum limit. In any case, much larger deviations are observed for the standard solution (19). Upon investigating the constancy of P_{xx} directly in Fig. 6(b), it is noticeable that deviations are present at the interface, unlike the constant P_{xx} observed for Q9 with high-isotropy-order interaction models [Fig. 5(c)]. This suggests that the high-order lattice models [Fig. 6(b)] do not satisfy mechanical equilibrium $dP_{xx}/dx = 0$, unlike those for Q9 [Fig. 5(c)]. Typical remedies for this type of issue include alteration of relaxation τ, spatial discretization, and interaction strengths, which produce different results, none of which, however, actually rectify the deviations observed. This is surprising given that c_s^2 (≈ 0.3675) for the Q25ZOT lattice is relatively close to c_s^2 (≈ 0.3333) for Q9. It was found that the deviations at the interface increased for lattices with larger c_s^2, such as Q49ZOTT (see Appendix A) and Q21 [56], which have twice, if not more, as large c_s^2 compared to Q9. To demonstrate that these inconsistencies observed at the interface are *independent* of the accuracy of Eq. (17), we run the same simulations for Q25ZOT using the

E12 interaction model and another known as Q17ZOT (for details refer to [48]). Note that the ZOT variants Q17ZOT and Q25ZOT, although constructed on a different basis, have the same accuracy and c_s. In addition to this, we also run the same simulations using Q49ZOTT but with its c_s^2 modified to match that of the ZOT lattices c_s^2 (≈ 0.3675), which can be achieved by changing its reference temperature $T_0 = c_s^2$ and recalculating its weights (see Appendix A). We also note that it was not possible to set c_s^2 in Q49ZOTT equal to that of Q9 due to instability. As can be seen in Fig. 6(b), the result for Q25ZOT with E12 has the lowest spatial deviation, although, despite using the same interaction model as Q9 in Fig. 5(c), it does not eradicate the deviations at the interface. Compared to the rest of the results, the difference in $\Delta P_{xx}\%$ is very small and is attributed to the difference in $\mathcal{C}_4$ in E12, which, according to the continuum analysis (29) and (30) and according to Eqs. (37) and (38), changes the surface tension. It can be seen in Fig. 6(b) that the high-order models Q25ZOT, Q17ZOT, and Q49ZOTT, with interactions directly on the lattice, have indistinguishable results. The same result, although not shown here, is obtained when running Q49ZOTT with full fourth-order equilibrium (6). These results are interesting since both E12 and Q49ZOTT share most of the same lattice velocities, which includes the unique conditions applied on $\hat{z} = 13$ [refer to details in Fig. 3 and Eq. (16)]. This demonstrates that the inconsistencies observed at the interface are not
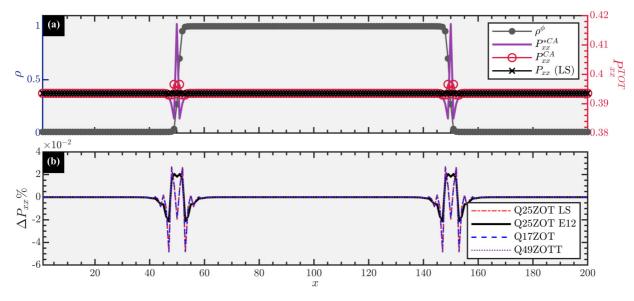
FIG. 6. Numerical results at equilibrium for the flat-interface test for a variety of lattice structures. (a) Pseudopotential interactions (11) are deployed directly on the Q25ZOT lattice structure. The interaction component of P_{xx}^{tot} obtained numerically P_{xx} (×) from Eq. (17) and its continuum approximation P_{xx}^{CA} (○) from Eqs. (29) and (30) are compared against the standard solution $P_{xx}^{*\text{CA}}$ (solid line) from Eq. (19). (b) Constancy $\Delta P_{xx}\%$ of the P_{xx} obtained numerically with Eq. (17) along spatial dimension x, tested for Q25ZOT on the LS and with E12, in addition to Q17ZOT and Q49ZOTT. Here, for Q49ZOTT, the sound speed c_s was modified to match that of the ZOT variants.

dependent on our proposed generalized solution (17). These inconsistencies observed at the interface are unexpected, in particular given that they are not resolved by usual means, as stated earlier. There is, after all, much more that is yet to be uncovered with the application of high-order lattices and perhaps the issue here is one of those. However, this requires further, and more dedicated, investigations, which we defer to future work. Nevertheless, it is clear from the above that these inconsistencies are independent of the accuracy of the solution from Eq. (17). To close, with Eq. (17) it is possible to obtain the exact interaction pressure for a variety of high-order lattice structures. While its continuum approximation (29) and (30) degrades in accuracy with increasing order of isotropy, it is consistently shown here to be the more accurate solution compared to Eq. (19). Considering, in addition, the continuum analysis in Sec. IV, it can be definitively concluded that the standard solution (19), even on standard lattices such as the Q9, does not accurately describe the pseudopotential interaction pressure tensor.

B. Spherical interface

We now move on to demonstrating the validity of our generalized interaction pressure tensor (17) where all possible symmetries can be considered, e.g., a spherical interface, using the single droplet test. Here we also consider a non-ideal fluid system that consists of two immiscible components ϕ and φ with dissimilar viscosities and all possible interactions included. We set $\rho_0^\phi/\rho_0^\varphi = 1$ and ensure that they are dissimilar fluids by $\tau^\phi \neq \tau^\varphi$ and as such simply set intra-interactions (self-interactions) $\mathcal{G}^{\phi\phi} = \mathcal{G}^{\varphi\varphi}$. Mutual inter-interactions (cross-interactions) require the condition that strengths $\mathcal{G}^{\phi\varphi} = \mathcal{G}^{\varphi\phi}$. Here we test the same lattices as previous tested, namely, Q9 on the lattice and with E8, E10, and E12, and high-order models: Q17ZOT, Q25ZOT, and

Q49ZOTT. In addition to these we also test the following common high-order lattices available from the literature: Q17 [8], Q21 [56], Q25 [11], and Q37 [46]. In addition, we run Q49ZOTT with its standard c_s and also with c_s modified to match the ZOT variants which we denote by Q49ZOTT*. In all tests, it was possible to keep $\tau^\phi = 0.9$ and $\tau^\varphi = 1.2$ for all lattices, except for Q25 due to its high value in c_s^2, which requires relaxation to be set to $\tau^\phi = 1.2$ and $\tau^\varphi = 1.6$. The pseudopotentials of inter- and intra-interactions are set to have the form $\psi(\rho) = \rho^0(1 - e^{-\rho/\rho^0})$ and $\Psi(\rho) = \rho$ for each respective fluid. Since all lattices were applied to the same computational domain, this meant that lattices with different sounds speeds do not correspond to the same physical reference, i.e., only in the case for ZOT lattice variants are sounds speeds the same. As such, different c_s required different surface tension. With τ fixed, simulations were ensured to remain stable by using $\mathcal{G}^{\phi\phi}$ and $\mathcal{G}^{\phi\varphi}$ to control the surface tension coefficient and interface width. We approximate for appropriate values of $\mathcal{G}^{\phi\phi}$ and $\mathcal{G}^{\phi\varphi}$ by first setting the (repulsive) cross-interaction strength $\mathcal{G}^{\phi\varphi}$ approximately at, or close to, the immiscible limit.[4] Depending on the stability, $\mathcal{G}^{\phi\varphi}$ was altered. Then the self-interaction strength $\mathcal{G}^{\phi\phi}$ was set so that the initial bulk pressure, in an *approximated* form, namely, $P_0^\phi = c_s^2 \rho^\phi + \mathcal{C}_2 \frac{\mathcal{G}^{\phi\phi}}{2}(\psi^\phi)^2 + \mathcal{C}_2 \frac{\mathcal{G}^{\phi\varphi}}{2}\Psi^\phi \Psi^\varphi$, is a nonzero positive value.

---

[4]The immiscible limit is defined when mutual diffusion is at zero or below, which, following [40], we approximated by $\mathcal{G}^{\phi\varphi} > \mathcal{G}_{\text{crit}}^{\phi\varphi} \approx c_s^2 4/\mathcal{C}_2[\rho_0^\phi + \rho_0^\varphi]$ (since $\Psi = \rho$) due to the explicit coupling of the forcing terms (4), (5), (7b), and (8). This is used purely as an indicator as it does not account for $\mathcal{G}^{\phi\phi}$. The main purpose of $\mathcal{G}^{\phi\phi}$ and $\mathcal{G}^{\phi\varphi}$ in the tests conducted here is to control the surface tension coefficient and stability.
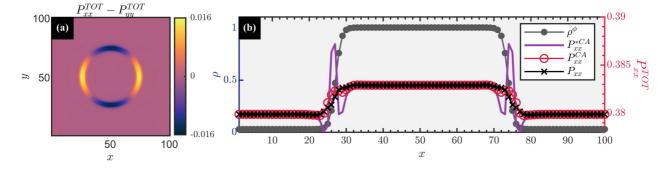
FIG. 7. Single static circular droplet results for Q49ZOTT* with modified c_s. (a) Mismatch between normal and tangential components of the total pressure tensor (9), (10), and (17). (b) Cross-sectional profiles along x at $y = n_y/2$, comparing the interaction component of P_{xx}^{tot} obtained numerically P_{xx} ($\times$) from Eq. (17), its continuum approximation P_{xx}^{CA} ($\circ$) from Eqs. (29) and (30), and the standard solution P_{xx}^{*CA} (solid line) from Eq. (19).

To ensure stable solutions the intra- and inter-interaction strengths for the different lattices are set, for Q9 (including on lattice, E8, E10, and E12), Q17, Q17ZOT, Q25ZOT, and Q49ZOTT*, to $\mathcal{G}^{\phi\phi} = -0.15046$ and $\mathcal{G}^{\phi\varphi} = 1.2$; for Q21, Q37, and Q49ZOTT, to $\mathcal{G}^{\phi\phi} = -1.0156$ and $\mathcal{G}^{\phi\varphi} = 1.8$; and for Q25, to $\mathcal{G}^{\phi\phi} = -1.3792$ and $\mathcal{G}^{\phi\varphi} = 2.2$. Note that we do not claim that the simulation parameters provide the optimal results, but that they are sufficient for the sake of testing the validity of Eq. (17).

We show the mismatch between the total pressure tensor components in Fig. 7(a), and in Fig. 7(b) the interface profiles are shown. We do not expect P_{xx} to be constant along the interface in Fig. 7(b) as there is now ambiguity in symmetry and because the inner and outer bulk phase densities are no longer the same, due to dissimilar viscosities and all interactions now being included. Nevertheless, we can see clearly in Fig. 7(b) that the numerical calculation (17) is far more uniform than its continuum approximation (29) and (30), although, again, we see that (29) and (30) are far more accurate than the standard solution (19), which suffers from large variations.

Furthermore, we assess the ability of our generalized discrete interaction pressure tensor (17) to reproduce the Laplace experiment, which defines the surface tension coefficient σ as the slope of the pressure difference ΔP as a function of the inverse radius, that is, $\Delta P = \sigma/R$. To conduct this test, an approximate theoretical surface tension coefficient σ is obtained by treating the problem as a one-dimensional problem [34,43], similar to the flat interface, where Eqs. (37) and (38) are then solved along x, at the horizontal cross section, allowing the Laplace ΔP to be evaluated for a range of R. We then directly test if Eq. (17) is able to reproduce the slope. A series of simulations is conducted independently for a range of R_0 where upon reaching equilibrium the actual R is measured. To compute ΔP we calculate the difference between the equation of state P_0 in the bulk of each fluid phase, i.e., $\Delta P = P_0^\phi - P_0^\varphi$. Since the total pressure tensor is isotropic ($P_N = P_T$) in the bulk of each phase, which is shown clearly in Fig. 7(a), this allows P_0 to be defined by Eq. (9), which consists of the kinetic contribution from Eq. (10) plus P_N^{int} from Eq. (17). Here we have used $P_N^{int} = P_{xx}^{int}$ for the sake of consistency. As we can see in Fig. 8, all 11 lattices tested are capable of reproducing the Laplace experiment. The theoretical approximations and the numerical results are in

excellent agreement with the percentage difference observed in Fig. 8 for all 11 lattices tested remained within less than $\pm 2.5\%$. The accuracy of the general interaction pressure tensor expression (17) is further appreciated in Fig. 8(b), where the results for both ZOT lattices and Q49ZOTT* are essentially the exact same. This is the same feature discussed earlier in the flat-interface test. For comparison, on the same plot we included results for Q17 where, due to a different c_s^2 ($\approx 0.370\,25$), have slightly different results but are still within close proximity to the ZOT lattices.

VI. CONCLUSION

We have derived a universal definition for the interaction pressure tensor for high-order lattice structures in line with the discrete theory by Shan [32]. We also derived a generalized form of its continuum approximation truncated at fourth-order-isotropy gradients. From this it was possible to demonstrate that thermodynamic consistency is satisfied on higher-order lattices using the pseudopotential proposed by Sbragaglia and Shan [36]. The discrete on-lattice interaction pressure tensor (17) and its continuum approximation (29) and (30) were validated against theory for the flat-interface and single-droplet test case for a variety of high-order lattice structures. These tests collectively confirm that our derived general expression (17) can accurately and consistently calculate the pressure tensor on high-order lattices. The current definition can be extended to consider lattices at higher orders by eliminating the limitation for symmetry groups of mixed components ($\hat{z}$) in Eq. (16). We point out that our method can already consider most common high-order lattice structures currently available from the literature. With our proposed generalized interaction pressure tensor it is possible to study complex fluid systems with higher-order lattices using pseudopotentials, such as viscous coalescence [57] of droplets and binary collisions of immiscible droplets [18]. With the interaction pressure tensor now more readily obtained for high-order lattices at the continuum limit (29) and (30), it is possible to define various other transport properties, such as the diffusion constants of and between various components. Such work would further broaden the applicability of high-order lattice models, in particular for microscopic fluid dynamic systems involving nonideal fluid mixtures.
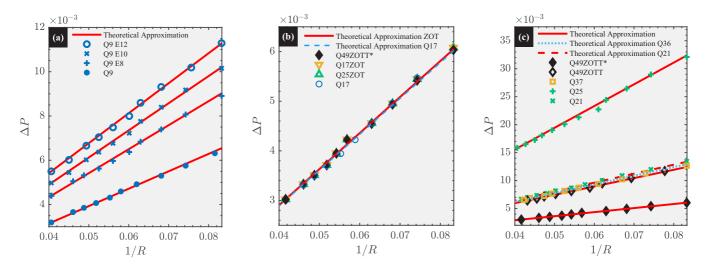
FIG. 8. Laplace experiment for the single static circular droplet test including intra- and inter-interactions for 11 different lattice models. The numerical results (symbols) are obtained by setting the initial R_0 [in Eq. (D2)] and then at equilibrium, by postprocessing, measuring the actual R and calculating the difference between the equation of state, computed by Eqs. (9) and (17), of the two bulk phases, i.e., $\Delta P = P_0^\phi - P_0^\varphi$. The theoretical approximations (lines) are obtained by computing σ from Eqs. (37) and (38), treated as a one-dimensional problem, using the density profiles from equilibrated numerical results (for each respective lattice) for the case $R \approx R_0 = 25$. The Laplace $\Delta P = \sigma/R$ is then solved for the range $R = 12, \ldots, 25$ directly using this approximated σ. For visual purposes, all 11 different lattices are presented over three plots (a-c) and theoretical approximations between different lattices are differentiated using solid, dashed, and dotted lines. Note in (b) the results for Q49ZOTT* (♦), both the theoretical approximation and the numerical, are the same as those presented in (c).

APPENDIX A: THE Q49ZOTT LATTICE STRUCTURE

The weights for D1Q7 constructed on the ZOTT $\{0, \pm 1, \pm 2, \pm 3\}$ lattice are given by [37]

$$w_{(0)} = \tfrac{1}{36}\left\{c_s^2\left[3\left(14 - 5c_s^2\right)c_s^2 - 49\right] + 36\right\},$$

$$w_{(\pm 1)} = \tfrac{1}{16}\left\{c_s^2\left[c_s^2\left(5c_s^2 - 13\right) + 12\right]\right\},$$

$$w_{(\pm 2)} = \tfrac{1}{40}\left\{c_s^2\left[5\left(2 - c_s^2\right)c_s^2 - 3\right]\right\},$$

$$w_{(\pm 3)} = \tfrac{1}{720}\left\{c_s^2\left[15\left(c_s^2 - 1\right)c_s^2 + 4\right]\right\} \tag{A1}$$

and the reference temperature

$$T_0 = \frac{2}{3} + \frac{1}{3}\sqrt[3]{\frac{7}{5(3\sqrt{30} - 5)}} - \frac{\sqrt[3]{\frac{5(3\sqrt{30}-5)}{7}}}{35^{2/3}}, \tag{A2}$$

where the sound speed is related by $T_0 = c_s^2$. We extend this to two dimensions using the idea that the number of lattice velocities is Q^D, where D is the number of spatial dimensions. Reconstructing the ZOTT D1Q7 lattice in two dimensions therefore require $7^2 = 49$ lattice velocities, which we can satisfy by utilizing the first three lattice sites as shown in Fig. 1. The weights (A1) are then extended into two dimensions by [37]

$$w_\alpha = w_{(\xi_{\alpha,i})} \times w_{(\xi_{\alpha,j})}. \tag{A3}$$

For example, the first two weights of Q49ZOTT in Fig. 1 are $w_{\alpha=0} = w_{(0)} \times w_{(0)}$ and $w_{\alpha=1} = w_{(1)} \times w_{(0)}$, and so on.

To impose conditions on the isotropy coefficients as done in main text, i.e., $\mathcal{C}_2 = 1$ and $\mathcal{C}_4 = c_s^2$, we require $\tilde{w}_\alpha = w_\alpha/c_s^2$. It is also possible to change T_0, which requires us to recalculate w_α from Eq. (A1).

APPENDIX B: LATTICE ISOTROPY

The isotropy orders ($m = 2n$, where n is a even integer) of the lattice structure are defined by

$$\sum_\alpha \tilde{w}_\alpha \xi_{\alpha,i}\xi_{\alpha,j}\xi_{\alpha,k}\cdots\xi_{\alpha,\mathcal{O}^m} = \mathcal{C}_m \triangle_{ijk\cdots\mathcal{O}^m}^{(m)},$$

where $\mathcal{C}_m$ is the constant for mth-order isotropy and $\triangle_{ij\cdots(\mathcal{O}^m)}^{(m)}$ is the product of standard Knocker delta functions δ_{ij} and is given by the recursion relation [52]. The orders are to be even, hence $2n$, since odd orders $(2n - 1)$ sum to zero,

$$\sum_\alpha \tilde{w}_\alpha \xi_{\alpha,i}\xi_{\alpha,j}\xi_{\alpha,k}\cdots\xi_\alpha^{(2n-1)} = 0,$$

and thus the isotropy is of order one $\sum_\alpha \tilde{w}_\alpha(\xi_{\alpha,x})^1 = 0$. The second-, fourth-, sixth-, and eighth-order isotropies are, respectively,

$$\sum_\alpha \tilde{w}_\alpha \xi_{\alpha,i}\xi_{\alpha,j} = \mathcal{C}_2\triangle_{ij}^{(2)} = \mathcal{C}_2\delta_{ij},$$

$$\sum_\alpha \tilde{w}_\alpha \xi_{\alpha,i}\xi_{\alpha,j}\xi_{\alpha,k}\xi_{\alpha,l} = \mathcal{C}_4\triangle_{ijlk}^{(4)} = \mathcal{C}_4(\delta_{ij}\delta_{kl} + \delta_{il}\delta_{kj} + \delta_{ik}\delta_{jl}),$$

$$\sum_\alpha \tilde{w}_\alpha \xi_{\alpha,i}\xi_{\alpha,j}\xi_{\alpha,k}\xi_{\alpha,l}\xi_{\alpha,m}\xi_{\alpha,n}$$

$$= \mathcal{C}_6\triangle_{ijlkmn}^{(6)} = \mathcal{C}_6(\delta_{ij}\delta_{kl}\delta_{mn} + \cdots),$$

$$\sum_\alpha \tilde{w}_\alpha \xi_{\alpha,i} \xi_{\alpha,j} \xi_{\alpha,k} \xi_{\alpha,l} \xi_{\alpha,m} \xi_{\alpha,n} \xi_{\alpha,s} \xi_{\alpha,q}$$

$$= \mathcal{C}_8 \triangle_{ijlkmnsq}^{(8)} = \mathcal{C}_8 (\delta_{ij} \delta_{kl} \delta_{mn} \delta_{sq} + \cdots).$$

Furthermore, isotropy orders beyond second order involve constraints due to increasing combination of tensors as shown above. On a two-dimensional square lattice with components $ijk \cdots q := x, y$, Sbragaglia *et al.* [43] showed that

$$\sum_\alpha \tilde{w}_\alpha (\xi_{\alpha,x})^{(2a)} (\xi_{\alpha,y})^{(2b)} = \mathcal{C}_{(2a+2b)} (2b-1)!! (2b-1)!!,$$

where $m = 2n = 2a + 2b$. For example, fourth-order isotropy ($m = 6$) satisfies the two constraints ($a = 2$ and $b = 0$)

$$\sum_\alpha \tilde{w}_\alpha \xi_{\alpha,x} \xi_{\alpha,x} \xi_{\alpha,x} \xi_{\alpha,x}$$

$$= \sum_\alpha \tilde{w}_\alpha (\xi_{\alpha,x})^4 = \mathcal{C}_4 (\delta_{xx} \delta_{xx} + \delta_{xx} \delta_{xx} + \delta_{xx} \delta_{xx}) = 3\mathcal{C}_4$$

and ($a = 1$ and $b = 1$)

$$\sum_\alpha \tilde{w}_\alpha \xi_{\alpha,x} \xi_{\alpha,x} \xi_{\alpha,y} \xi_{\alpha,y} = \mathcal{C}_4.$$

Due to the fixed condition $\mathcal{C}_2 = 1$ set here, we conveniently have $\mathcal{C}_4 = c_s^2$. The isotropy constraints are best assessed without a dependence on $\mathcal{C}_m$, which can be done using basic algebra (for more details see [43])

$$\frac{\sum_\alpha \tilde{w}_\alpha (\xi_{\alpha,x})^4}{\sum_\alpha \tilde{w}_\alpha \xi_{\alpha,x} \xi_{\alpha,x} \xi_{\alpha,y} \xi_{\alpha,y}} = 3.$$

Moreover, higher isotropy orders, for example, sixth order $m = 6$, satisfy the two constraints ($a = 3$ and $b = 0$)

$$\sum_\alpha \tilde{w}_\alpha (\xi_{\alpha,x})^6 = 15\mathcal{C}_6$$

and ($a = 2$ and $b = 1$)

$$\sum_\alpha \tilde{w}_\alpha (\xi_{\alpha,x})^4 (\xi_{\alpha,y})^2 = 3\mathcal{C}_6$$

such that

$$\frac{\sum_\alpha \tilde{w}_\alpha (\xi_{\alpha,x})^6}{\sum_\alpha \tilde{w}_\alpha (\xi_{\alpha,x})^4 (\xi_{\alpha,y})^2} = 5.$$

Using details provided in Appendix A, the high-order lattice model Q49ZOTT, illustrated in Fig. 1, can be shown to completely satisfy these fourth- and sixth-order isotropy constraints.

APPENDIX C: INTERACTION PRESSURE TENSOR ON THE EIGHT-ORDER ISOTROPY LATTICE STRUCTURE

To demonstrate that Eqs. (15) and (16) conform with the methodology in [32], we show the pressure tensor in its expanded form. To do this, we neglect all cross-interaction terms $\mathcal{G}^{\phi\varphi} = 0$. For the sake of brevity, a single-component case is considered and we drop the component-specific superscript $\psi = \psi^\phi$ and $\mathcal{G} = \mathcal{G}^{\phi\phi}$. In addition, we consider the same two force interaction vectors as done in [32], namely, a purely axial vector $\boldsymbol{\xi} = (2, 0)$ and mixed component vector $\boldsymbol{\xi} = (2, 1)$, which correspond to symmetry groups $\bar{z} = 4$ and $\hat{z} = 5$, respectively.

For the vector $\boldsymbol{\xi}_\alpha^{\bar{z}=4} = (2, 0)$, in Eq. (15) the variables have the value $\mathcal{E}^{\bar{z}=4} = \max_\alpha (|\boldsymbol{\xi}_\alpha^{\bar{z}=4}|) = 2$, which leads to a total of $2 - 1 = 1$ additional contribution (and thus $\beta = 1$). Since $\boldsymbol{\varepsilon}_\beta^{\bar{z}=4} = \mathbf{U} \circ \mathrm{sgn}(2, 0) = (1, 0)$ we identify that $\boldsymbol{x} + \boldsymbol{\varepsilon}_\beta^{\bar{z}=4} = \boldsymbol{x} + \boldsymbol{\xi}_\alpha^{\bar{z}=4}/2$ and $\boldsymbol{x} - \boldsymbol{\xi}_\alpha^{\bar{z}=4} + \boldsymbol{\varepsilon}_\beta^{\bar{z}=4} = \boldsymbol{x} - \boldsymbol{\xi}_\alpha^{\bar{z}=4}/2$, and thus Eq. (15) will reduce to

$$\mathcal{P}_{ij}^{\bar{z}=4}(\boldsymbol{x}) = \frac{\mathcal{G}}{4} \psi(\boldsymbol{x}) \sum_\alpha \left[\tilde{w}_\alpha \psi(\boldsymbol{x} + \boldsymbol{\xi}_\alpha^{\bar{z}=4}) \right] \xi_{\alpha,i}^{\bar{z}=4} \xi_{\alpha,j}^{\bar{z}=4} + \frac{\mathcal{G}}{4} \sum_\alpha \left[w_\alpha \psi\left(\boldsymbol{x} + \frac{\boldsymbol{\xi}_\alpha^{\bar{z}=4}}{2}\right) \psi\left(\boldsymbol{x} - \frac{\boldsymbol{\xi}_\alpha^{\bar{z}=4}}{2}\right) \right] \xi_{\alpha,i}^{\bar{z}=4} \xi_{\alpha,j}^{\bar{z}=4}. \tag{C1}$$

For the vector $\boldsymbol{\xi}_\alpha^{\hat{z}=5} = (2, 1)$, in Eq. (16) we still have $\mathcal{E}^{\hat{z}=5} = 1$ and now the directional unit vector is equal to $\boldsymbol{\varepsilon}_\beta^{\hat{z}=5} = \mathbf{U} \circ \mathrm{sgn}(2, 1) = (1, 1)$. If we consider the center point $\boldsymbol{x} = (0, 0)$, then $\boldsymbol{x} + \boldsymbol{\varepsilon}_\beta^{\hat{z}=5} = (1, 1)$ and $\boldsymbol{x} - \boldsymbol{\xi}_\alpha^{\hat{z}=5} + \boldsymbol{\varepsilon}_\beta^{\hat{z}=5} = (-1, 0)$. Expanding the sum of interactions for the entire symmetry group $\hat{z} = 5$, Eq. (16) reduces to (using the same α index as in Fig. 2 in [32])

$$\mathcal{P}_{ij}^{\hat{z}=5}(\boldsymbol{x}) = \frac{\mathcal{G}}{4} \psi(\boldsymbol{x}) \sum_\alpha \left[\tilde{w}_\alpha \cdot \psi(\boldsymbol{x} + \xi_\alpha^{\hat{z}=5}) \right] \xi_{\alpha,i}^{\hat{z}=5} \xi_{\alpha,j}^{\hat{z}=5} + \frac{\mathcal{G}}{4} \tilde{w}_\alpha \times \left\{ [\psi(1,1)\psi(-1,0)] \xi_{17,i} \xi_{17,j} + [\psi(1,1)\psi(0,-1)] \xi_{18,i} \xi_{18,j} \right.$$

$$+ [\psi(-1,1)\psi(0,-1)] \xi_{19,i} \xi_{19,j} + [\psi(-1,1)\psi(1,0)] \xi_{20,i} \xi_{20,j} + [\psi(-1,-1)\psi(1,0)] \xi_{21,i} \xi_{21,j}$$

$$+ \left. [\psi(-1,-1)\psi(0,1)] \xi_{22,i} \xi_{22,j} + [\psi(1,-1)\psi(0,1)] \xi_{23,i} \xi_{23,j} + [\psi(1,-1)\psi(-1,0)] \xi_{24,i} \xi_{24,j} \right\}. \tag{C2}$$

Comparing the above directly with equations in [32], Eq. (C1) is essentially the same as Eq. (18) and (C2) is the combined form of Eqs. (19) and (20).

APPENDIX D: INITIAL DENSITY PROFILES

The initial density profiled for the flat-interface and single-droplet test in Sec. V was set using a hyperbolic tangent function [20]. For the flat interface, we set ρ^ϕ as the inner fluid with thickness $n_x/2$ placed in the center by setting $x_{\min} = n_x/4$ and $x_{\max} = 3n_x/4$ using the function

$$\rho^\phi(x, y) = \rho_0^\phi \left\{ c_L + \frac{c_H - c_L}{2} \left[\tanh\left(\frac{2(x - x_{\min})}{W_0} \right) \right. \right.$$

$$\left. \left. - \tanh\left(\frac{2(x - x_{\max})}{W_0} \right) \right] \right\}$$

and then set ρ^φ as the outer portion by

$$\rho^\varphi(x,y) = \rho_0^\varphi \left\{ c_H + \frac{c_L - c_H}{2} \left[\tanh\left(\frac{2(x - x_{\min})}{W_0} \right) \right.\right.$$
$$\left.\left. - \tanh\left(\frac{2(x - x_{\max})}{W_0} \right) \right] \right\}, \tag{D1}$$

where W_0 is the interface width. We denote the upper and lower concentrations by c_H and c_L, which are set to $c_H = 1$ and $c_L = 1 \times 10^{-4}$ (the standard application of the LB method requires $c_L \neq 0$). The variables ρ_0^ϕ and ρ_0^φ denote the initial densities.

Similarly, for the single-droplet test, the droplet with radius R centered at $\boldsymbol{x}$ is initialized by

$$\rho^\phi(x,y) = \frac{\rho_0^\phi}{2} \left\{ (c_H + c_L) - (c_H + c_L) \tanh\left(\frac{2(R^* - R_0)}{W_0} \right) \right\}$$

and the surrounding fluid by

$$\rho^\varphi(x,y) = \frac{\rho_0^\varphi}{2} \left\{ (c_L + c_H) - (c_L + c_H) \tanh\left(\frac{2(R^* - R_0)}{W_0} \right) \right\}, \tag{D2}$$

where R_0 is the initial radius and $R^* = \sqrt{(x - x_0)^2 + (y - y_0)^2}$ with the location of the droplet defined by coordinates x_0 and y_0. In this test the droplet is placed in the center $x_0 = n_x/2$ and $y_0 = n_y/2$.

[1] G. Whitesides, Nature (London) **442**, 368 (2006).
[2] N. Pamme, Lab Chip **6**, 24 (2006); D. Pappas, Analyst **141**, 525 (2016); N.-T. Nguyen, M. Hejazian, H. C. Ooi, and N. Kashaninejad, Micromachines **8**, 20 (2017).
[3] C. Aidun and J. Clausen, Annu. Rev. Fluid Mech. **42**, 439 (2010).
[4] L. Bocquet and P. Tabeling, Lab Chip **14**, 3143 (2014).
[5] J. Zhang, Microfluid. Nanofluid. **10**, 1 (2011).
[6] M. Bernaschi, S. Melchionna, S. Succi, M. Fyta, E. Kaxiras, and J. Sircar, Comput. Phys. Commun. **180**, 1495 (2009).
[7] S. Succi, Philos. Trans. R. Soc. A **374**, 20160151 (2016).
[8] X. Shan, X.-F. Yuan, and H. Chen, J. Fluid Mech. **550**, 413 (2006).
[9] H. Chen and X. Shan, Physica D **237**, 2003 (2008).
[10] J. Meng and Y. Zhang, Phys. Rev. E **83**, 036704 (2011).
[11] P. C. Philippi, L. A. Hegele, L. O. E. dos Santos, and R. Surmas, Phys. Rev. E **73**, 056702 (2006).
[12] M. R. Swift, W. R. Osborn, and J. M. Yeomans, Phys. Rev. Lett. **75**, 830 (1995).
[13] X. Shan and H. Chen, Phys. Rev. E **47**, 1815 (1993).
[14] I. V. Karlin, A. Ferrante, and H. C. Öttinger, Europhys. Lett. **47**, 182 (1999).
[15] B. M. Boghosian, J. Yepez, P. V. Coveney, and A. Wager, Proc. R. Soc. A **457**, 717 (2001).
[16] S. S. Chikatamarla, C. E. Frouzakis, I. V. Karlin, A. G. Tomboulides, and K. B. Boulouchos, J. Fluid Mech. **656**, 298 (2010).
[17] A. Mazloomi M, S. S. Chikatamarla, and I. V. Karlin, Phys. Rev. Lett. **114**, 174502 (2015).
[18] M. Wöhrwag, C. Semprebon, A. Mazloomi Moqaddam, I. Karlin, and H. Kusumaatmaja, Phys. Rev. Lett. **120**, 234501 (2018).
[19] L. Chen, Q. Kang, Y. Mu, Y.-L. He, and W.-Q. Tao, Int. J. Heat Mass Transf. **76**, 210 (2014).
[20] H. Huang, M. Krafczyk, and X. Lu, Phys. Rev. E **84**, 046710 (2011).
[21] M. L. Porter, E. T. Coon, Q. Kang, J. D. Moulton, and J. W. Carey, Phys. Rev. E **86**, 036701 (2012).
[22] S. Galindo-Torres, A. Scheuermann, L. Li, D. Pedroso, and D. Williams, Comput. Phys. Commun. **184**, 1086 (2013).

[23] B. Dollet, A. Scagliarini, and M. Sbragaglia, J. Fluid Mech. **766**, 556 (2015).
[24] S. Varagnolo, D. Ferraro, P. Fantinel, M. Pierno, G. Mistura, G. Amati, L. Biferale, and M. Sbragaglia, Phys. Rev. Lett. **111**, 066101 (2013).
[25] S. Varagnolo, V. Schiocchet, D. Ferraro, M. Pierno, G. Mistura, M. Sbragaglia, A. Gupta, and G. Amati, Langmuir **30**, 2401 (2014).
[26] D. Lycett-Brown, I. Karlin, and K. H. Luo, Commun. Comput. Phys. **9**, 1219 (2011).
[27] X. Shan and H. Chen, Phys. Rev. E **49**, 2941 (1994).
[28] X. Shan and G. Doolen, J. Stat. Phys. **81**, 379 (1995).
[29] X. Shan and G. Doolen, Phys. Rev. E **54**, 3614 (1996).
[30] R. Benzi, M. Sbragaglia, S. Succi, M. Bernaschi, and S. Chibbaro, J. Chem. Phys. **131**, 104903 (2009).
[31] B. Derjaguin and N. Churaev, J. Colloid Interface Sci. **66**, 389 (1978).
[32] X. Shan, Phys. Rev. E **77**, 066702 (2008).
[33] M. Sbragaglia, R. Benzi, M. Bernaschi, and S. Succi, Soft Matter **8**, 10773 (2012).
[34] M. Sbragaglia and D. Belardinelli, Phys. Rev. E **88**, 013306 (2013).
[35] A. Montessori, G. Falcucci, M. La Rocca, S. Ansumali, and S. Succi, J. Stat. Phys. **161**, 1404 (2015).
[36] M. Sbragaglia and X. Shan, Phys. Rev. E **84**, 036703 (2011).
[37] S. S. Chikatamarla and I. V. Karlin, Phys. Rev. E **79**, 046701 (2009).
[38] X. He, X. Shan, and G. D. Doolen, Phys. Rev. E **57**, R13 (1998).
[39] X. Shan, Phys. Rev. E **81**, 045701(R) (2010).
[40] K. Küllmer, A. Krämer, W. Joppich, D. Reith, and H. Foysi, Phys. Rev. E **97**, 023313 (2018).
[41] T. Krüger, F. Varnik, and D. Raabe, Phys. Rev. E **79**, 046704 (2009).
[42] M. Gross, N. Moradi, G. Zikos, and F. Varnik, Phys. Rev. E **83**, 017701 (2011).
[43] M. Sbragaglia, R. Benzi, L. Biferale, S. Succi, K. Sugiyama, and F. Toschi, Phys. Rev. E **75**, 026702 (2007).
[44] R. Ramadugu, S. P. Thampi, R. Adhikari, S. Succi, and S. Ansumali, Europhys. Lett. **101**, 50006 (2013).
[45] J. H. Irving and J. G. Kirkwood, J. Chem. Phys. **18**, 817 (1950).
[46] X. Shan and H. Chen, Int. J. Mod. Phys. C **18**, 635 (2007).

[47] X. Shan, Phys. Rev. E **73**, 047701 (2006).

[48] X. Shan, Phys. Rev. E **81**, 036702 (2010).

[49] X. Shan, IMA J. Appl. Math. **76**, 650 (2011).

[50] S. S. Chikatamarla and I. V. Karlin, Phys. Rev. Lett. **97**, 190601 (2006); Comput. Phys. Commun. **179**, 140 (2008).

[51] R. Benzi, L. Biferale, M. Sbragaglia, S. Succi, and F. Toschi, Phys. Rev. E **74**, 021509 (2006).

[52] S. Wolfram, J. Stat. Phys. **45**, 471 (1986).

[53] L. Biferale, P. Perlekar, M. Sbragaglia, and F. Toschi, Commun. Comput. Phys. **13**, 696 (2013).

[54] J. G. Kirkwood and F. P. Buff, J. Chem. Phys. **17**, 338 (1949).

[55] J. S. Rowlinson and B. Widom, *Molecular Theory of Capillarity* (Clarendon, Oxford, 1982).

[56] R. Zhang, X. Shan, and H. Chen, Phys. Rev. E **74**, 046703 (2006).

[57] M. Gross, I. Steinbach, D. Raabe, and F. Varnik, Phys. Fluids **25**, 052101 (2013).